NASA CR-72763

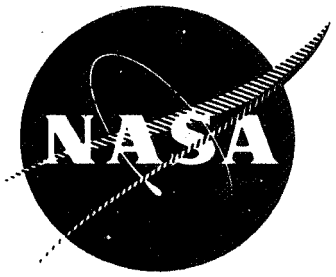

DEVELOPMENT OF Cr-Li-Y_2O_3 COATINGS FOR CHROMIUM-BASE ALLOYS

by

J.W. Clark

GENERAL ELECTRIC COMPANY

prepared for

NATIONAL AERONAUTICS AND SPACE ADMINISTRATION

NASA-Lewis Research Center
CONTRACT NAS 3-11174
John P. Merutka, Project Manager
Joseph R. Stephens, Research Advisor

NASA CR-72763

FINAL REPORT

DEVELOPMENT OF Cr-Li-Y_2O_3 COATINGS FOR CHROMIUM-BASE ALLOYS

by

J.W. Clark

GENERAL ELECTRIC CO.
Evendale, Ohio 45215

prepared for

NATIONAL AERONAUTICS AND SPACE ADMINISTRATION

February 5, 1971

CONTRACT NAS 3-11174

Technical Management
NASA-Lewis Research Center
Cleveland, Ohio 44135
John P. Merutka, Project Manager
Joseph R. Stephens, Research Advisor

TABLE OF CONTENTS

LIST OF ILLUSTRATIONS

LIST OF ILLUSTRATIONS (Concluded)

LIST OF TABLES

ABSTRACT

This report presents results of the evaluation of Li-doped, Y_2O_3-stabilized Cr_2O_3 surface layers as a means of increasing the resistance of Cr-base alloys to embrittlement in air oxidation, as measured by a change in ductile-brittle transition temperature. The plasma-sprayed chromium plus 10 volume percent Y_2O_3 was the most effective of several coatings studied.

1.0 SUMMARY

This work was undertaken to develop a coating system capable of preventing the drastic embrittlement suffered by chromium-base alloys during air exposure at elevated temperatures. The approach selected for evaluation was treatment of the alloy surface to produce a stable, adherent, low-ionic-defect Cr_2O_3 or complex oxide with Cr_2O_3. A stabilized form of the natural oxidation product of chromium was pursued by:

(1) doping with monovalent Li,

(2) adding significant volume fractions of Y_2O_3 particles to surface regions,

(3) pretreatment in pure oxygen to affect partial conversion to complex oxides, and

(4) combinations of these approaches.

The metalliding* process, which produces diffusion coatings by electrolysis in a fused salt bath, was used in producing Li and Cr + Li surface layers. Plasma spraying was employed to deposit Cr + Y_2O_3 coatings containing from 10 to 50 volume percent of the oxide.

The best system identified was made by first chromiding at low current density in a LiF-CrF_3 bath, followed by plasma spraying of a Cr + 10 volume percent Y_2O_3 powder mixture and preoxidation in pure oxygen. The ductile-brittle transition temperature (DBTT) of the substrate was 580°F; this was increased by no more than 100°F by 200-hour 2100°F air exposures of coated samples, when such exposures were performed isothermally or under cyclic conditions in which moderate rates of cooling to room temperature at specified intervals (360°F per minute) were employed. However, when initial cooling rates during cyclic air exposure were increased to 960°F per minute, considerable blistering of the scales resulted and the DBTT increased to about 900°F. Although this is a marked improvement over the DBTT value of well above 1400°F exhibited by the noncoated alloy after much less severe air exposures (and appears to be at least equivalent to any other known coating for Cr), it does not seem to provide adequate protection for jet engine service.

*Metalliding is a highly proprietary process, licenses for which are available from General Electric's Patent and Technology Marketing Operation in Schenectady, New York.

2.0 INTRODUCTION

The continued development of high-temperature chromium-base alloys, conducted by this laboratory for the past three years under NASA sponsorship, has produced compositions with tensile strengths on the order of 50,000 psi and 100-hour rupture strengths of over 15,000 psi at 2100°F. These alloys thus offer an increase of 250 to 300°F over the temperatures at which equivalent strengths are attained by the most advanced superalloys in current use in advanced air-breathing engines. Chromium alloys of this general strength level, after surface conditioning and annealing, exhibit tensile ductility of about 5% RA at temperatures as low as 350°F; but, their ductility drops rapidly at lower temperatures. Furthermore, embrittlement during air oxidation can raise the ductile-brittle transition temperature (DBTT) to much higher values. This embrittlement, which is common to virtually all chromium alloys, is due primarily to reaction with nitrogen. Although the inherent oxidation resistance of chromium is one of the major factors in the continued interest in this metal as an alloying base, the unmodified surface scales are not sufficiently protective to prevent ingress of nitrogen during protracted exposure at elevated temperatures. For this reason, coatings (or more precisely, surface protection systems) will be required for any extended application of chromium alloys in advanced engines.

The embrittlement problem has not been completely solved in high-strength-alloy systems through compositional modifications. Alloying additions of monovalent solutes such as Li, and of certain rare earth and related elements (e.g., La, Y, Ce), are effective in retarding interaction with N_2 by virtue of promoting more stable surface scales. These nitridation-inhibiting solutes are difficult to add to an alloy by conventional melting techniques because of their restricted solubility and high reactivity with oxygen present in the melt and in the ceramic crucibles employed in induction melting. Furthermore, when successfully added in amounts sufficient to provide increased oxidation resistance, such solutes usually have detrimental effects on bulk-dependent properties such as strength and ductility due to segregation in the ingot. This is particularly true of rare earth or monovalent metal additions, which concentrate in grain boundaries and dendritic intersticies during freezing and result in hot shortness at fairly low alloy contents. It would be advantageous to restrict these elements to surface regions of high strength alloys. As will be described in detail in later sections, this has been the major approach followed in the development program herein. Before proceeding with a description of the coating systems evaluated in this work, it is appropriate to review briefly the oxidation behavior of chromium and chromium alloys.

2.1 CHROMIUM OXIDATION

Unalloyed chromium exhibits low oxidation kinetics in terms of weight gain in oxygen and air[1,2], but reaction with nitrogen can produce contamination leading to appreciable embrittlement of any chromium-base component. Both the oxidation and nitridation processes of unalloyed chromium are extremely complex and can, for instance, be affected by surface preparation[2], gas velocity[3,4] and the structure and working history of the material[2,5]. Although the detailed mechanism(s) through which these variations occur are not known, a qualitative understanding of some of thes observations can be suggested by considering that Cr_2O_3 grows by cation diffusion and that above about 1800°F Cr_2O_3 transforms to CrO_3 which is a volatile meastable oxide[6,7]. The presence of high residual stresses in the growing Cr_2O_3 film can induce oxide cracking and exfoliation, a step which many investigators regard as being a prerequisite to nitrogen contamination. The nitrogen contamination of chromium is often associated with a loose and nonadherent oxide.

There can be little doubt that the most serious effect of air exposure is nitrogen contamination, and that nitrogen is the most detrimental interstitial contaminant[8-10]. The critical nitrogen content, above which the transition temperature of unalloyed chromium is markedly increased, may be as low as 2 ppm for extruded rod in tension and as high as 100 ppm for cast chromium in bending[8]. Oxygen is much less embrittling. As much as 3,400 ppm oxygen have been shown to have no serious effect on the transition temperature of as-cast chromium[8], and similar data have been generated for wrought and recrystallized materials[11]. It has been pointed out, however, that the tolerable oxygen level in chromium may well be below the range which has so far been investigated [a possibility that appears to be supported by the identification of grain-boundary Cr_3O_4 particles in iodide chromium with 30 to 50 ppm oxygen[12]]. The effect, if any, of oxygen is much less detrimental than that of nitrogen.

Fortunately, the effects of interstitials on the transition temperature, and particularly the effects of nitrogen, are sensitive to working and heat treatment. It is generally acknowledged that nitrogen in solution is more deleterious than nitrogen pinned at dislocations or precipitated as Cr_2N. Slow cooling, to precipitate dissolved interstitials, has been found to produce a 270°F reduction in the transition temperature of 290 ppm N_2 material[8]. Even the ductility of material with only 10 ppm N_2 can be promoted by slow cooling rather than quenching after heat treatment at 2732°F[12]. Cold working increases the tolerable limit for nitrogen from about 10 to about 200 ppm[8,13].

Although heat treatment can be used to control the effect of dissolved nitrogen in chromium-base materials, exposure in air will (in time) produce a surface layer of Cr_2N whose gross effect on ductility cannot be controlled

through processing. A layer of nitride only 1 to 5 x 10^{-4} inch thick (as produced by heating unalloyed chromium in air for 200 hours at 1740°F) can produce an increase in DBTT of at least 400°F. Similarly, the exposure of a simple Cr-(Zr, Ti)C composition for 16 hours at 2000°F to produce a Cr_2N layer of 5 x 10^{-4} inch thick will raise the DBTT by about 1000°F[14], while a 100-hour exposure of a stronger Cr-W-(Zr, Ti)C composition at 1600 to 1800°F can increase the DBTT by as much as 1500°F[5]. It is this drastic embrittlement that must be prevented if chromium alloys are ever to be considered for significant application as high-temperature structural materials.

2.2 OXIDATION CR/RARE-EARTH ALLOYS

Considerable work has been reported over the past several years on alloying additions to prevent nitrogen contamination and embrittlement. In general, rare earths, Y, and the Group IVA metals have been documented to have a beneficial effect on nitridation resistance when added to unalloyed chromium[15,16]. More detailed studies on complex alloys have shown yttrium and lanthanum to be the preferred additions. Figure 1 presents a plot of weight gain and depth of nitride thickness observed on simple Cr-Y binary alloys after 2300°F/100-hour air exposure, indicating that a yttrium addition of 0.6 to 0.8 wt. % is required to prevent nitridation for this time-and-temperature condition. Complex alloys exhibit incipient melting and hot shortness at considerably lower Y concentrations. The maximum solubility of yttrium in chromium has been reported to be about 0.9 wt. % at 2260°F[17]. More recent investigations, however, have indicated much lower solubility. The addition of most solutes decreases the solubility of Y still further, and produces hot shortness during working and/or high-temperature brittleness in the fabricated composition. In the higher-strength alloys, such as the Cr-Mo-TaC composition that was coated in the present study, ductility and fabricability limitations dictate a maximum yttrium level of about 0.2 wt. %. Although this level of yttrium addition controls the rate of nitridation at temperatures of about 1800°F, it is not effective throughout the temperature range of interest. It is evident, therefore, that yttrium additions per se cannot be relied upon for the complete elimination of nitrogen-induced embrittlement in complex chromium materials. Indeed, in certain carbide-strengthened alloys the presence of fairly large concentrations of elemental yttrium, though beneficial at higher temperatures, appears to increase embrittlement in the lower temperature region[5].

As a portion of our work on Contract NAS3-7260, a number of additional reactive metals were evaluated with respect to their effect on the nitridation resistance of a binary Cr alloy containing 4 atomic percent Mo[14]. Since they closely resemble Y, emphasis was placed on the lighter rare earths from the lanthanide and actinide series, including mischmetal which is a naturally-occurring mixture of the elements in the first portion of the former series.

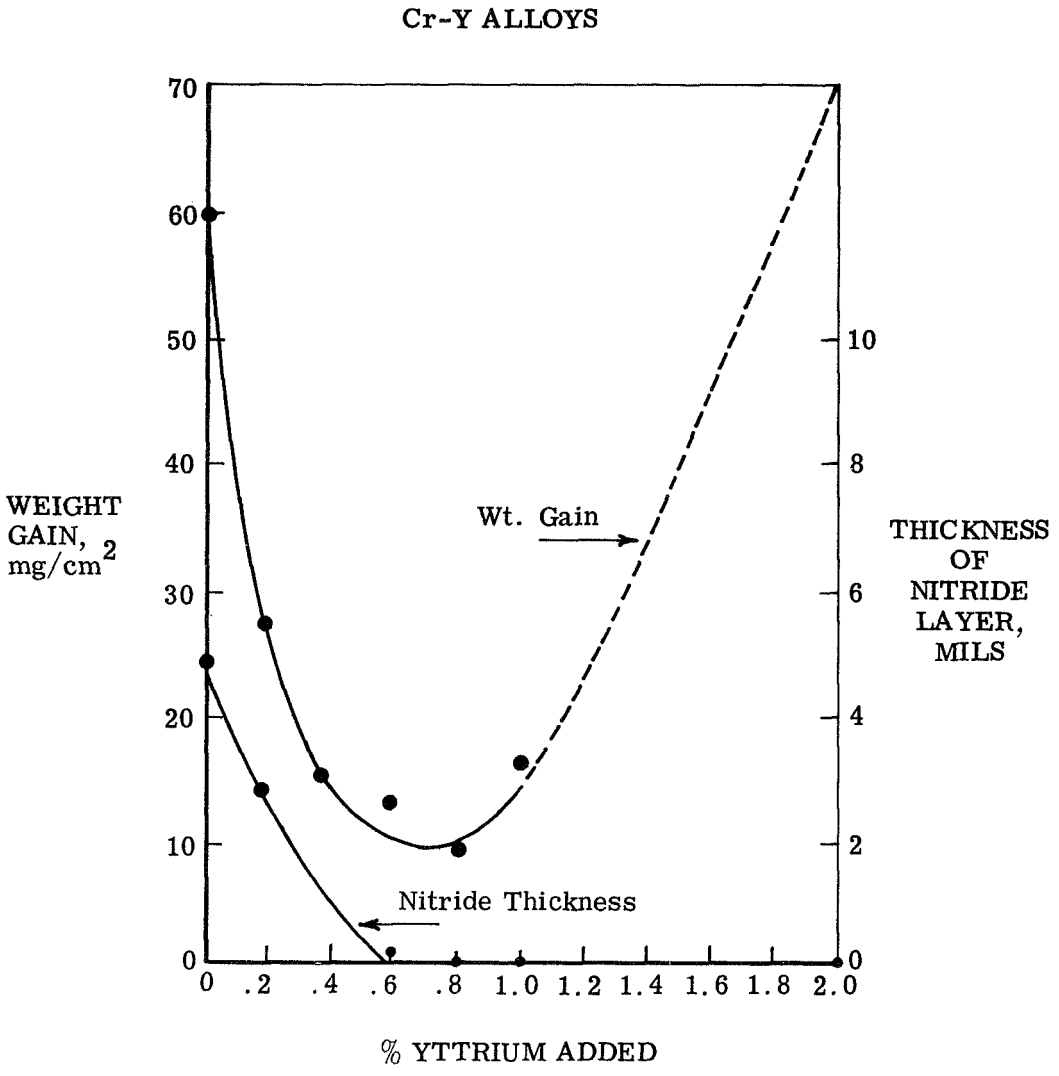

Figure 1. Effect of Yttrium Additions on the Weight Gain and Depth of Cr_2N after 100-Hour Exposure at 2300°F.

It was found that additions of La and Pr are more effective than Y in improving the air-oxidation resistance of the Cr-4Mo base and that additions of mischmetal are at least equivalent. Additions of 0.5 atomic percent lanthanum or praseodymium to the Cr-4Mo alloy completely prevent nitridation in 24-hour air exposure at 2400°F. Some minor agglomeration of the second phase, which is presumed to be rich in the rare-earth metal, is observed in the alloys with Pr additions; but, the Cr-Mo-La alloy is virtually unchanged from the as-cast condition. No evidence of incipient melting at 2400°F was detected with rare-earth additions.

In an effort to elucidate the mechanisms through which the rare-earth metals exert their beneficial effects on air oxidation of Cr, warm-rolled specimens of a binary Cr-0.2La alloy were recrystallized by annealing in vacuum at 2100°F for 1 hour, then electropolished and exposed to air at 2100°F for 10 minutes, 1 hour, 10 hours, and 100 hours. The specimens were mounted and polished with a 5:1 taper such that an additional five-fold magnification of the surface scale and subscale was imposed upon the optical magnification selected for examination. Taper sections after air exposures of 1 hour and 100 hours are shown in Figure 2. No evidence of a nitride layer was observed in any of the specimens. After the shorter-time exposure, there appears to be some porosity in the outer portions of the oxide; but, that portion closest to the oxide-metal interface is quite dense and protrudes prominently into the matrix at more or less regular intervals. After 100 hours at 2100°F, two distinct oxide phases are observed, with much more porosity evident in the outer scale. In most regions, the darker underlying oxide seems to be continuous, but there are areas in which the lighter, porous oxide is in contact with the matrix. Back reflection X-ray patterns from the scale(s) in each specimen yielded only lines which could be indexed as slightly contracted Cr_2O_3, with a_o = 4.953A, and c_o = 13.584A. However, in electron microprobe scans of the specimen exposed for 100 hours, the intensity of the La emission increased by a factor of 15 to 18 at the position of the darker, inner oxide in Figure 2 compared to the La intensity level in the general matrix. This suggests that formation of a complex oxide such as $LaCrO_3$ has taken place after 100 hours. Both Seybolt[18,19] and Hagel[1] have observed such phases in studies of Cr alloys containing additions of rare-earth metals or oxides.

Sheet samples of the same Cr-0.2La alloy were exposed to air oxidation for 2,900 hours at 2000°F and then tested without any surface conditioning in three-point bending over a radius of 4t. The DBTT increased from the original value of about 0°F in the rolled-and-annealed condition to only about 200°F after this rather severe oxidation. No nitride formation was detected, and the scale was extremely tenacious. It is therefore clear that the rare-earth metals can be, at least in simple alloys, quite effective over protracted periods of time. In chromium alloys containing carbides, the superiority of La over other rare earths in promoting oxida-

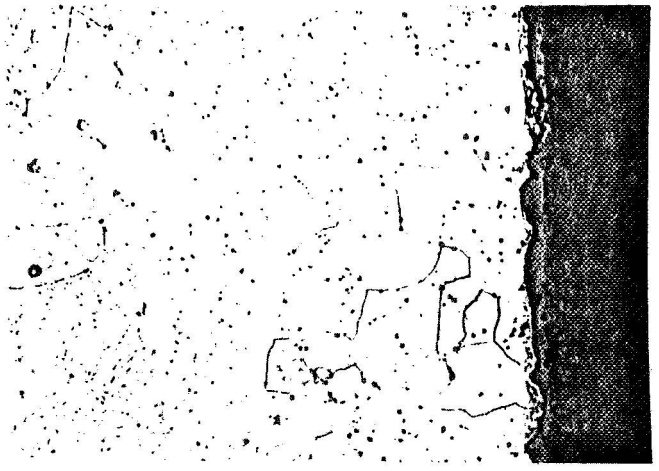

A. 1 Hour at 2100°F, 250X
5:1 Taper M5084

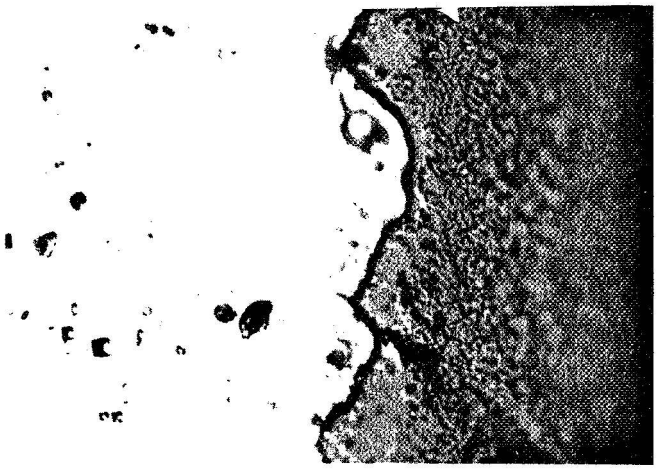

B. 1 Hour at 2100°F, 1000X
5:1 Taper N991

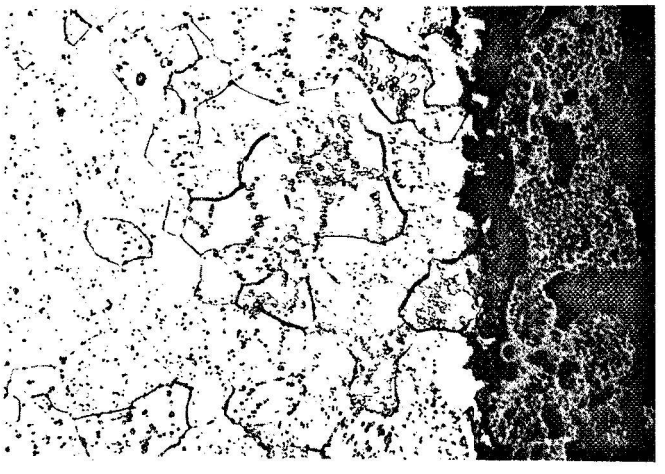

C. 100 Hours at 2100°F, 250X
5:1 Taper M5081

Figure 2. Taper Sections through Surface Scales Formed on Cr-0.2La Alloy after 2100°F Air Exposure.

tion resistance was even more pronounced, but larger additions were required. Incipient melting was observed at the effective concentration of 0.5 atomic percent at 2100°F in alloys produced from moderate-purity chromium and of 0.2 atomic La at 2000°F in alloys from high-purity iodide chromium. These observations are intended to point out that, in evaluating the effects of rare-earth metals on both oxidation properties and melting behavior, the form in which such elements are present must be considered. It appears likely that in alloys made from lower purity Cr, a large part of the La may have been tied up as interstitial compounds, probably oxides, since this is the major impurity. In this form, incipient melting is of course not a problem. In addition, these related data indicate that rare-earth concentrations of the same general magnitude are equally effective in promoting oxidation and nitridation resistance of a given alloy base regardless of the form in which they are initially present. As the matrix becomes complex, the required rare-earth concentration is reduced. These points are critical to one of the approaches emphasized in the present study.

2.3 OXIDATION OF CR ALLOYS CONTAINING RARE-EARTH OXIDES

Seybolt[18,19] has shown in studies at the GE Research and Development Center that the oxidation/nitridation resistance of a Cr-5^{v}/o Y_2O_3 alloy produced by powder-metallurgy techniques is comparable and, in some respects, superior to that observed by others in Cr-Y or Cr-La alloys[1,5,15,16]. As shown in Figure 3, the oxidation rates at both 2100 and 2280°F became markedly lower than parabolic after 3 hours exposure. The oxide scales which formed in 100 hours were tightly adherent even upon very rapid air cooling. This is often enough to completely shatter the scale from cooling samples of pure chromium or many chromium alloys. In addition, no nitrides were formed at either temperature. In contrast, rates of weight gain in air at 2500°F remained parabolic for 100 hours, and rather heavy Cr_2N layers were formed on both the Cr-5^{v}/o Y_2O_3 alloy and on pure chromium. In pure chromium at this temperature, oxidation weight gains decrease from parabolic; and, under some conditions, show a loss due to oxidation of surface Cr_2O_3 to the volatile species CrO_3 as recently developed in detail by Tedmon[7].

It is thus clear that the Y_2O_3 effect, while inoperative at 2500°F, is quite effective at and below 2300°F and that the improved air oxidation resistance conferred by Y_2O_3 cannot be accounted for simply by dissolved Y_2O_3 in Cr_2O_3 changing the diffusion rate of the rate-controlling Cr^{+3} ion. If this were the case, the kinetic data should still be parabolic, the only difference compared to pure chromium being a reduced rate constant. Neither is it tenable to suggest that the reduced weight-gain rate in Cr-Y_2O_3 is due to enhanced formation of the metastable CrO_3 (or in effect volatilizing

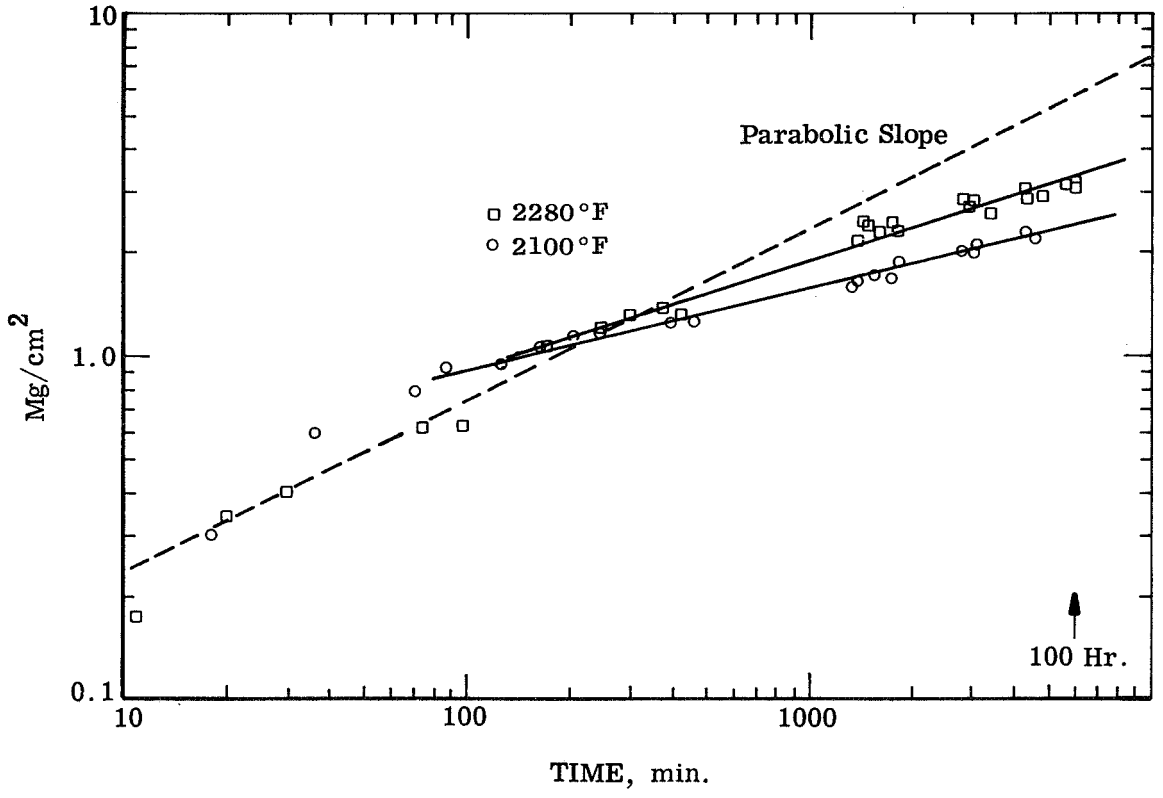

Figure 3. Weight Gain-Time Curves for Oxidation of Cr-5v/o Y_2O_3 in Air.

away some of the Cr_2O_3 layer by formating a gaseous oxide). As pointed out above, the weight-gain rate of the yttria-containing alloy was parabolic at 2500°F, i.e., the rate of weight gain was faster than that of unalloyed chromium at the higher temperature. On the other hand, it was observed in this and earlier work[1,18] that there is some formation of the perovskite oxide $YCrO_3$ during elevated temperature exposure, as well as dissolution of up to 1.5 mole percent Y_2O_3 in the Cr_2O_3 scale. As discussed by Seybolt[19], it seems likely that below 2300°F yttrium alters the nature of the Cr_2O_3-Y_2O_3 scale or the oxide-matrix interface.

A barrier, becoming increasingly effective with time, that tends to block the transfer of chromium into the Cr_2O_3 might offer an explanation of the observed kinetics. The following seems like a feasible mechanism. Assume that matrix Y_2O_3 and Cr_2O_3 scale react directly to form $YCrO_3$. This can happen even if the Cr_2O_3 solid solution is saturated with Y_2O_3. Since each mole of Y_2O_3 used forms two moles of $YCrO_3$, there is an appreciable increase in $YCrO_3$ content with time at the interface. The $YCrO_3$ (being depleted in chromium with respect to the pure chromium matrix) continuously reduces the diffusion flux of Cr^{+3} through Cr_2O_3, because the concentration gradient of migrating Cr^{+3} ions is reduced. Therefore, the slowly accumulating $YCrO_3$ at the Cr_2O_3/matrix interface tends to choke off the Cr_2O_3 growth. Since maintenance of a thinner scale tends to prevent exfoliation or cracking, this sequence of events would also be expected to result in the observed elimination of nitridation which appears, in all work on chromium or its alloys, to require direct access of nitrogen to the matrix through scale discontinuities. It is further possible that mechanical properties such as plasticity or strength of the scale are favorably altered by dissolution of Y_2O_3 in the Cr_2O_3, or that Y_2O_3 particles act as sinks for vacancies which would otherwise condense into voids that eventually lead to separation of the scale. Whatever the mechanism(s) involved, it is well demonstrated that Y_2O_3 dispersions lead to greatly-enhanced air oxidation resistance of chromium. With reference to coating considerations, it is likely that higher volume fractions than the $5^v/o$ of rare-earth oxides in the surface regions could lead to still further increases in protectiveness and stability.

2.4 OXIDATION OF CR/MONOVALENT-SOLUTE ALLOYS

The oxidation behavior of one further class of chromium alloys should be considered here. The oxide Cr_2O_3 is a "p" type semiconductor which forms during oxidation by diffusion of Cr^{+3} ions through the equilibrium concentration of cation vacancies in the lattice. If lower valence ions, particularly monovalent ions such as Li^+, or Na^+, or K^+, are added to Cr_2O_3 to replace Cr^{+3} ions in the lattice, the concentration of vacancies must decrease to maintain electrical neutrality. With this decrease, the diffusivity of Cr^{+3} (and, consequently, the parabolic-rate constant in

oxidation) should decrease accordingly. Early work by Hagel[1] showed this to be the case with trace additions of Li. By vapor depositing a film of Li on pure chromium prior to oxidation in both oxygen and air, k_p was reduced by a factor of about 15 over the temperature range of 1500 to 2200°F. We have shown in this laboratory that the mechanism is applicable to complex chromium alloys and, further, that it markedly reduces nitridation. A low-Y heat of the C-207 alloy (Cr-7.5W-0.8Zr-0.2Ti-0.1CY) was exposed in air for 50 hours at 2200°F with and without Li doping. The results are shown below:

Test No.	Amount of Li Initially Present	Weight Gain (mg/cm^2)	Depth Continuous Nitride	Depth GB Nitride
C-507	None*	54.0	15 mils/side	To 120 mils
C-501	Trace**	5.0	None	Virtually none
C-502	0.06 mg/cm^2***	0.5	None	Possible traces
C-504	0.10 mg/cm^2***	1.80	None	Possible traces

* Tested in clean system in which no Li runs had been performed.
** Tested in system in which Li-treated samples had been previously tested but with no intentional addition.
***Li added by dipping sample in saturated aqueous solution of Li_2CO_3 at room temperature.

One of the major difficulties in adding Li to chromium alloys is that its boiling point (about 2425°F) is well below the melting point of chromium. Although it has been possible to charge small amounts of Li to Fe-Cr alloys by melting under argon pressurization of about 10 atmospheres, the quantity and distribution were quite difficult to control. Thus, several means of enriching surfaces in Li, such as the two cutlined above, have been emphasized in preference to alloying.

More recently, Tedmon and Hagel have shown that effective lithided surfaces can be produced by electrodeposition on cathodic samples from a fused-salt electrolyte in the "Metalliding" processing[20,21]. Large improvements in oxidation rates afforded by such lithided surfaces are illustrated in Figure 4. Note that the parabolic rate k_p of the lithided sample is reduced by about two orders of magnitude below that of pure chromium. Similar reductions in oxidation rates were measured in air. These improvements are achieved by thin lithium-enriched layers, most in the range of about 0.9 mils. Although nitridation was not completely eliminated at and above 2200°F in air, only isolated patches of Cr_2N were observed; and, these appeared to be associated with blisters in the scale. In areas free of such blisters, no nitrides were detected.

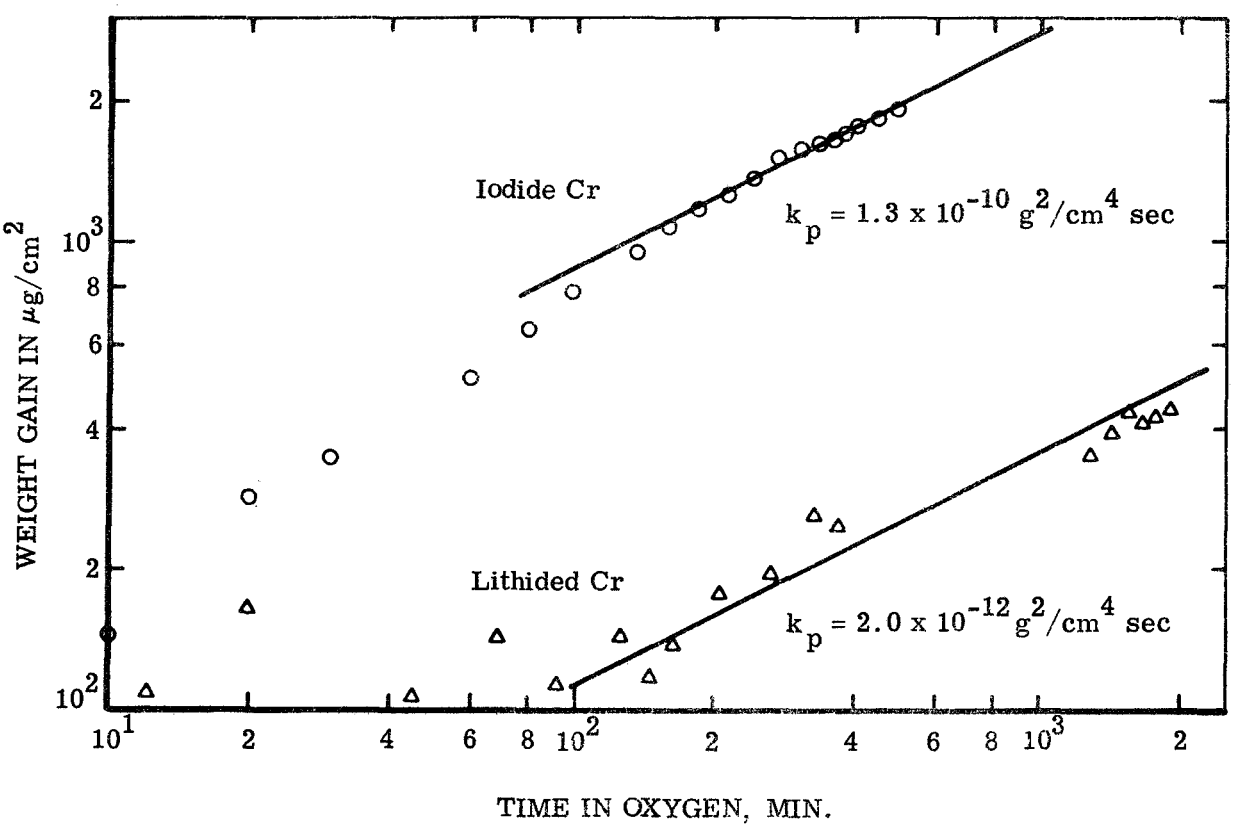

Figure 4. Oxidation Kinetics of Lithided Chromium and Pure Chromium at 2192°F.

Sufficient data have been accumulated to suggest that very small concentrations of Li are required. The exact electronic defect structure of Cr_2O_3 is unknown; but, it is clear, from both oxidation[1,2] and thermoelectric[22,23] measurements, that it is weakly "p" type with only slight cation deficiency (i.e., a low concentration of cation vacancies). Predominant valence is, of course, three; but, there may be transference to Cr^{+4} and Cr^{+6} at higher temperatures[6]. Incorporation of a monovalent alkali metal in the lattice would thus annihilate from two to five cation vacancies. Work by Hagel on the electrical conductivity of Li- substituted Cr_2O_3[24] indicates that only about 1.5 to 2.5 mole percent Li_2O (0.2 weight % Li) is required to increase the conductivity by an order of magnitude. Since the cation vacancy concentration is initially quite low, and the somewhat larger alkali metal ions (0.78A for Li^+ vs. 0.65A for Cr^{+3} and 1.32A for $O^{=}$) could be considered as still less mobile than chromium ions, a small level of Li in Cr alloys should permit attainment of this concentration in the oxide at the oxidation rate controlling site (the oxide-metal interface). In support of this point of view are the very large improvements observed in the oxidation behavior of the Cr-W-ZTC alloy when exposed in a furnace in which previous Li-doped runs had been made and the striking reductions in rate associated with lithided layers of only about 0.4-mil thickness.

In addition to the lithiding development outlined previously, it has recently been shown in proprietary work that trace amounts of Li can be codeposited with Cr under certain conditions when chromiding from a LiF metalliding cell. Thus, there are available methods of concentrating Li in narrow layers on a chromium alloy substrate, and of applying a dilute addition of Li at the same time that heavier Cr layers are deposited. The latter method has the advantage of isolating the reactive phases in the substructure (e.g., TaC in the alloy to be coated in the subject program) from the oxidizing surface, and may also provide a more effective reservoir of Li than would lithiding per se.

3.0 SELECTION OF COATING SYSTEM

There are, in quite general terms, two concepts that can be applied to the surface protection of alloys for use in corrosive environments. One is to so treat the surface that the stability of the natural reaction product(s) of the alloy in the particular environment is sufficiently enhanced to permit service under the imposed conditions. The other, and more common, approach is to overlay the surface with less reactive elements or compounds such that the identity of the reaction product(s) is completely changed to a more corrosion-resistant form. Approaches that were felt to be the most promising examples of each concept were considered for development and evaluation in this study, with the choice narrowed to one concept as outlined herein.

In order to successfully develop coatings for chromium, as for any other alloy base, it is necessary to consider carefully the mechanisms involved in the type of corrosion which must be prevented. This has been done in some detail in the foregoing sections. To review briefly, there are at least three independent mass transport mechanisms that are operative during reaction of chromium with the major components of air:

1) Cationic diffusion of Cr^{+3} through Cr_2O_3 toward the oxide-gas interface

2) Diffusion of nitrogen (and, but to less detrimental effect, oxygen) anions toward the oxide-chromium interface

3) Further oxidation of surface Cr_2O_3 to CrO_3 and the volatilization of the latter

It should also be pointed out again that nitridation, at least in the sense of the formation of continuous layers of the nitride Cr_2N, is not observed when the outer Cr_2O_3 scale is adherent and nonporous. Hagel[5] has shown that the diffusion rates of anions through Cr_2O_3 are slower than cations by a factor of at least 10^4; and, thus, one would not expect nitrogen diffusion through a growing, adherent scale. Formation of nitrides, on the other hand, invariably accompanies gross spalling or blisters of the Cr_2O_3. Since air is thereby admitted to the fresh Cr surface, the fact that nitridation now proceeds in preference to the oxidation that would seem to be expected, presents something of a dilemma unless, as suggested by Chang, the more reactive Cr-rich Cr_2O_3 near the metal interface acts as an oxygen "filter". However, the observation that nitride layers are associated with spalling or blistered oxide scales is well documented. Spalling is usually to be expected at some point in the oxidation of chromium, since the ratio of the specific volume on the oxide to

that of the metal forming it (the Pillings-Bedworth ratio) is over 1.0. Compressive stresses are thus generated in the oxide and eventually lead to buckling if the scale thickness reaches a critical value that is dependent upon temperature and imposed thermal stresses. Counteracting this buckling tendency at higher temperatures is the fact that Cr_2O_3, a volatile species, and the scale thickness is therefore maintained at a lower value than would otherwise be the case. If the rate of CrO_3 removal can be maintained at a low enough level, the volatilization could thus be beneficial in a surface protection system based on Cr_2O_3.

Since all evidence indicates that chromium oxidation proceeds by diffusion of Cr^{+3} through cation vacancies, lower-valent solutes in the oxide should be effective in slowing the reaction and thereby decreasing the tendencies to effoliate and admit nitrogen. Experiments with Li^+ have shown this to be the case. Mechanisms through which rare earths improve air-oxidation resistance are not fully established; as outlined previously, the improvements afforded by rare-earth additions are well documented and appear to arise from increased adherence of the oxide and a decreasing flux of Cr^{+3} ions through the growing scale. These beneficial effects are associated with favorable interactions between Cr_2O_3 and the rare earths in the form of oxides rather than in the elemental form. Keying of the Cr_2O_3 by rare-earth oxide [$(RE)_2O_3$] particles; interaction of $(RE)_2O_3$ and Cr_2O_3 to form perovskite oxides of the type $(RE)CrO_3$, which have higher thermal stability than the normal surface scale; changes in the strength and plasticity of Cr_2O_3 by minor dissolution of the rare earths; $(RE)_2O_3$ particles acting as sinks for vacancies that diffuse countercurrent to Cr atoms, thus retarding void formation and eventual spalling at the oxide-metal interface, have been advanced as models as discussed in preceding sections. All may, in fact, be involved to greater or lesser degrees.

Based on the factors summarized above, the requirements of this coating program can be stated as the development of a surface protection system that will prevent air embrittlement of chromium alloys without itself increasing the DBTT or decreasing the elevated-temperature strength. The system thus selected was derived from the point of view that the most effective coating for chromium alloys will be an adherent, stable, low-ionic-defect form of Cr_2O_3. This stabilized form of the natural oxidation product has been pursued by:

(1) Doping with monovalent Li

(2) Adding significant volume fractions of $(RE)_2O_3$ particles to surface regions

(3) Pretreatment of the coated alloy in pure oxygen to convert the rare-earth solutes to their oxides

(4) A combination of these approaches

This stabilized Cr_2O_3 approach was selected in preference to application of intermetallic coatings, primarily because most of the metals that might be considered as constituents of a coating are known either to drastically embrittle chromium or to greatly decrease its load-carrying capability at elevated temperatures. Large increases in DBTT are observed upon moderate addition of aluminum, of nickel, and (perhaps to a lesser degree) of silicon to chromium-base alloys. Additions of rare-earth elements, on the other hand, cause hot shortness at quite low concentrations. It would appear from available data that silicides offer the highest potential of any of the possible intermetallic systems, and recent work by Stephens[25] on such coatings is rather encouraging. However, it appeared at the outset of this work that stabilized Cr_2O_3 coatings offered a more promising approach than any intermetallic.

It is fully recognized that the stabilized-oxide approach represents a marked departure from usual coating processes. In chromium, the reaction rate in air is controlled by the diffusion of cations (predominately Cr^{+3}) through the growing scale. As long as that scale remains adherent, foreign anions such as nitrogen are denied access to the substrate, since their diffusion rates are lower than that of Cr^{+3} by a factor of at least 10^4. It was on this concept that the work described here has been based.

The specific surface coatings evaluated in this study are as follows:

(1) Li-doped Cr

(2) Y_2O_3 particles in Cr

(3) Preoxidation to form stabilized Cr_2O_3 and/or $YCrO_3$

(4) Combinations of the above

The metalliding process was used in producing Li and Cr+Li surface layers, and plasma spraying was employed to deposit $Cr+Y_2O_3$ coatings containing from 10 to 50 volume percent of the oxide. The coating techniques are described in following sections.

4.0 EXPERIMENTAL PROCEDURES

4.1 COATING TECHNIQUES

4.1.1 Metalliding

Metalliding is a process to produce diffusion coatings on metallic substrates by electrolysis in fused-salt baths[26]. This process encompasses the interaction, mostly in the solid state, of approximately 50 metals and metalloids ranging from beryllium to uranium. Over 400 combinations, not including alloy variations, have been studied using 20 different metals as anodes and over 40 as cathodes. The process is shown schematically in Figure 5. It is operated at temperatures ranging from about 900 to over 2200°F, using inert atmospheres and metallic reaction vessels. The coulombic yields are usually quantitative, particularly when the cathodic and anodic materials are rather widely separate in the electromotive series, and coating times are generally short. Controlled, uniform coatings ranging in thickness from a fraction of a mil to many mils can be obtained, many of which are unavailable by any other technique. This technique was used in the present work to produce chromium and lithium surface-alloying of a Cr-7Mo-2Ta-0.1C-0.13 (Y+La) substrate alloy.

A cross-sectional view of the type of laboratory-sizes electrolytic cell used is shown in Figure 6. It holds from 20 to 30 pounds of salt. The furnace is sealed except for a Fiberfrax gasket around the cell, so that the desired atmosphere can be maintained at all times. Purified argon was used in this study, although forming gas ($90\%N_2$, $10\%H_2$) is usually employed if the substrate being coated is insensitive to these gases. Nickel-plated steel covers for the Monel cells are water cooled and are fitted with electrically-insulated doors. Glass electrode towers, with gas inlet tubes for flushing when they are opened, are mounted to the cover plate with silicone rubber gaskets. Automatic regulation of the heat, flow meters for gases, and instrumentation for controlling and measuring electrolysis are provided on a control panel. A photograph of the two-cell station used in this work is shown in Figure 7. Cells of this type have now been in continuous use for over four years.

Most of the metalliding reactions function as batteries. Thus, many of the reactions are self-sustaining; but, generally, an external EMF is applied to secure higher and more-uniform current densities than the battery action will provide. In addition to using anodes of the metal to be deposited, shielded carbon anodes can also be used if the metalliding ion is replenished as it is consumed. This procedure was employed in the lithiding portion of the present work. Operating voltages become considerably higher with a carbon anode than with a metal anode.

A typical voltage plot is shown in Figure 8, which demonstrates that the potential differences are very low and can be used as a means of matching deposition to diffusion rates. If plating is building up on the surface, the return of the voltage to a negative-anode polarity upon interruption

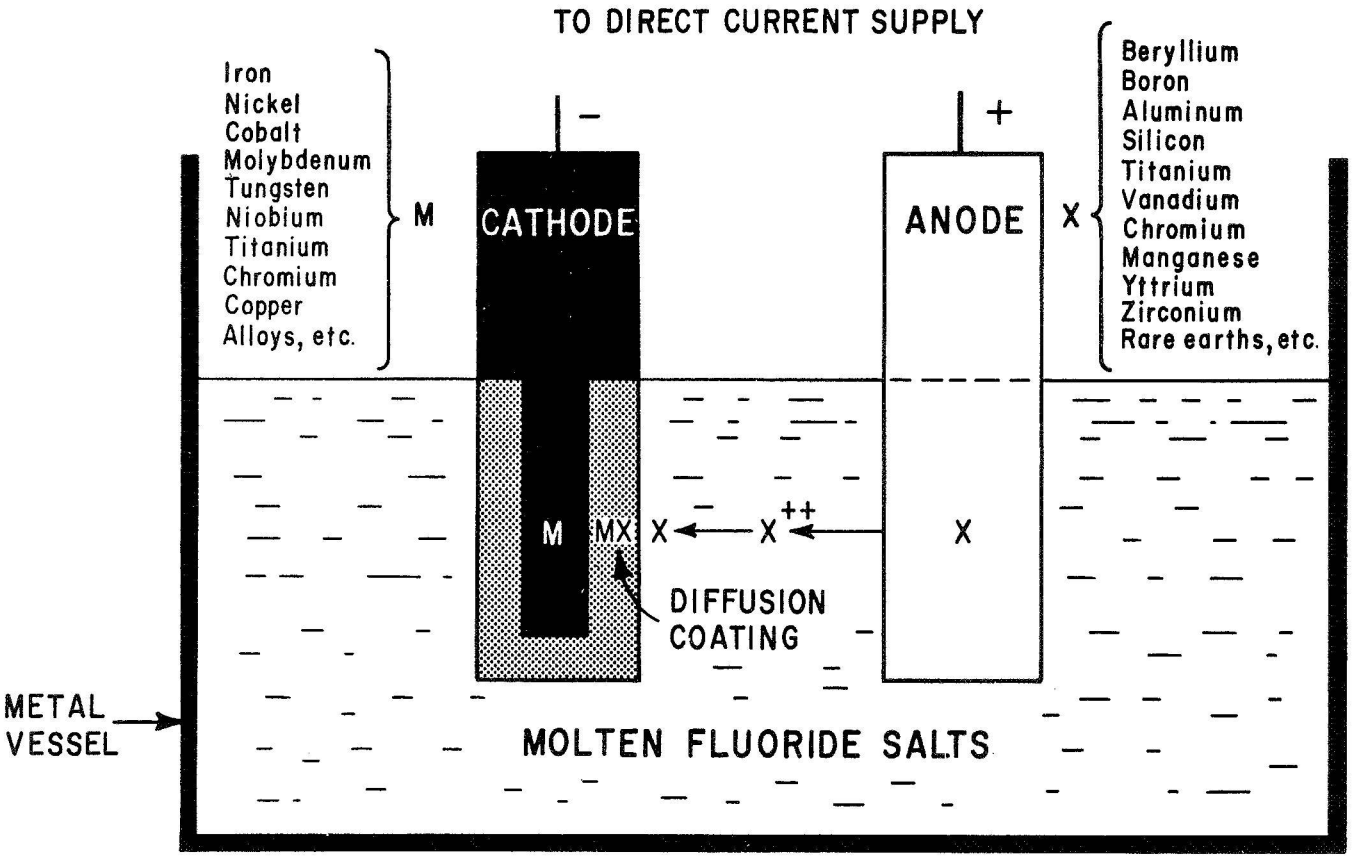

Figure 5. Schematic Representation of the Metalliding Process.

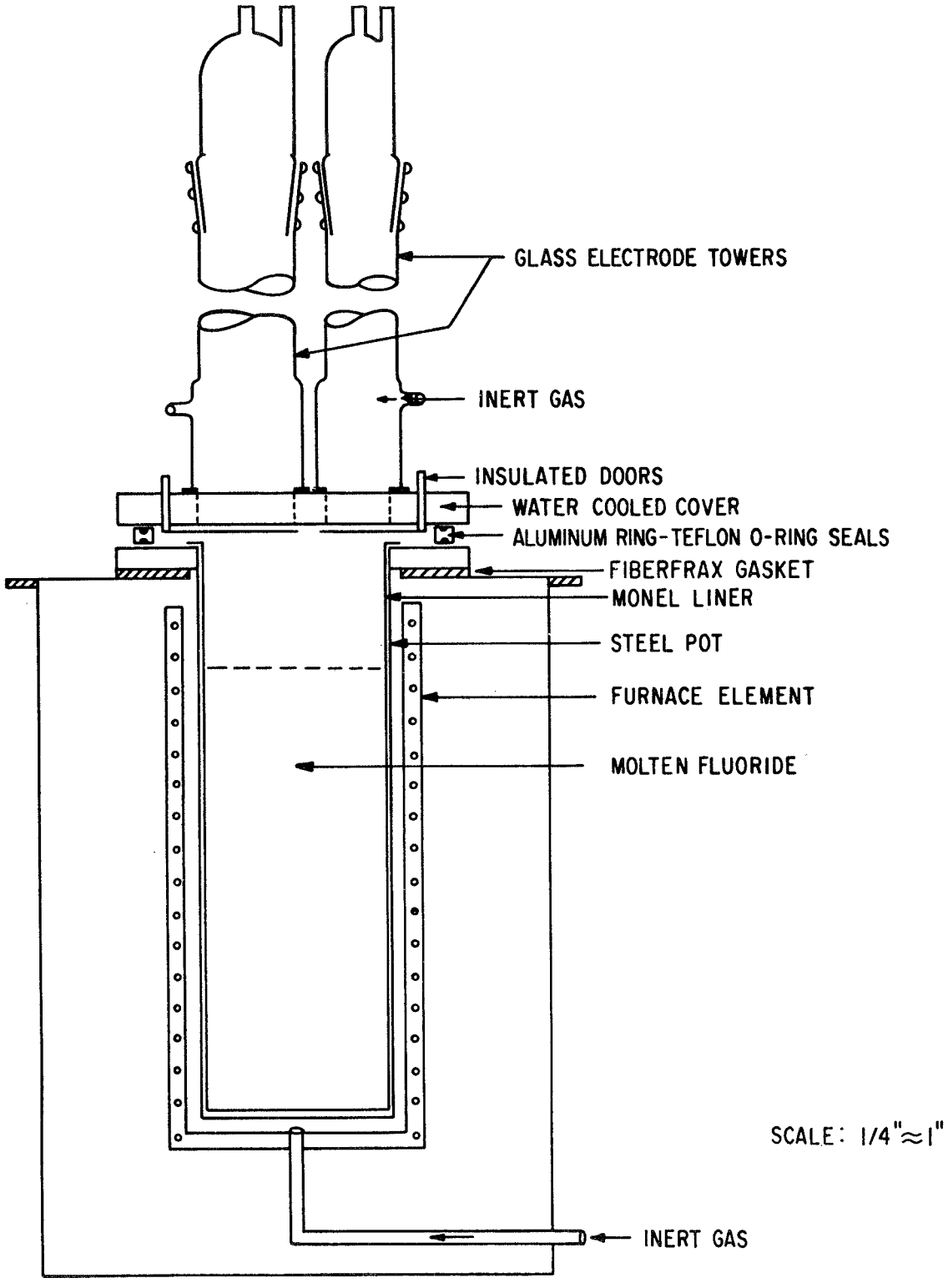

Figure 6. Cross Section of a Laboratory Metalliding Cell.

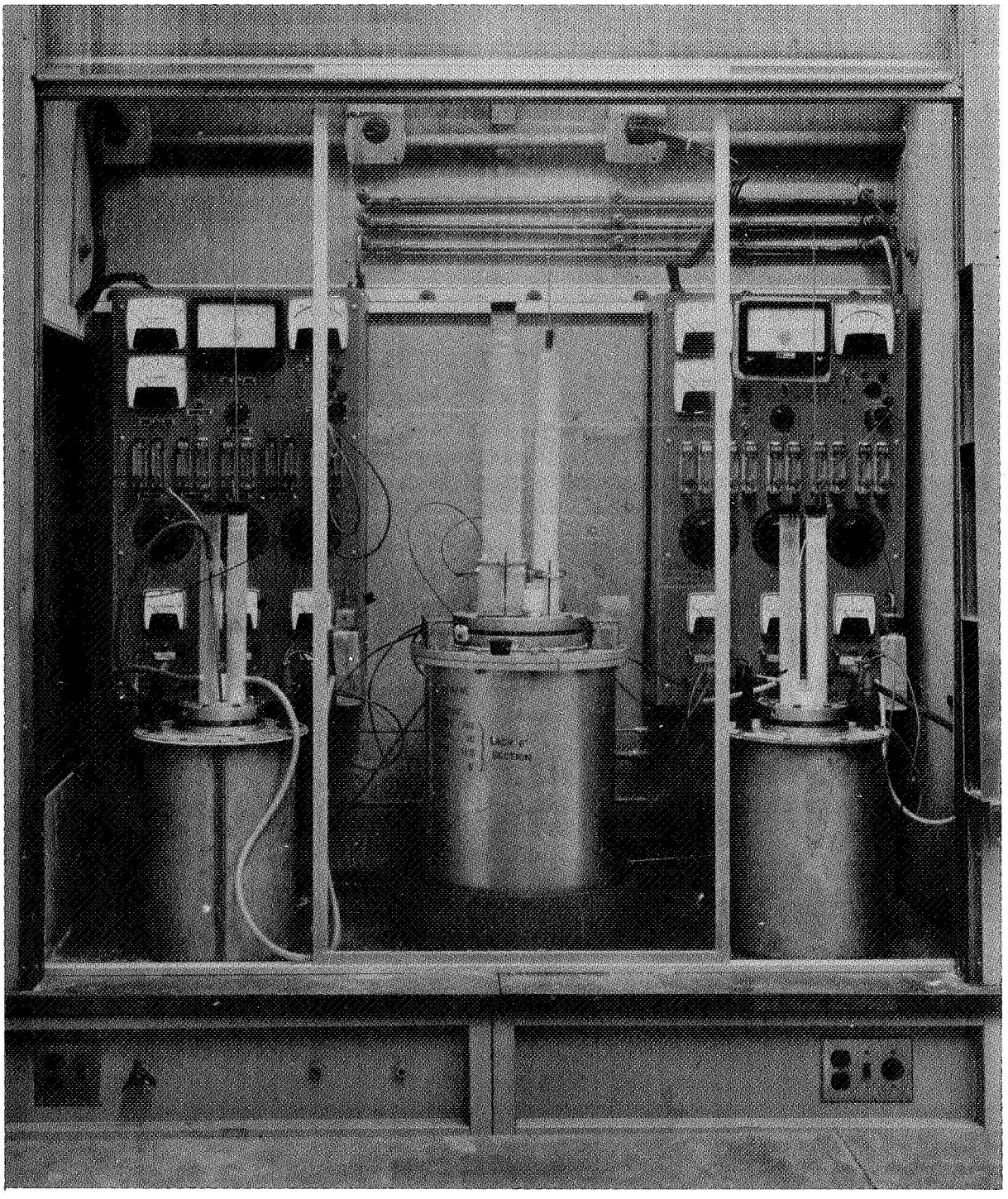

Figure 7. Typical Metalliding Cells and Related Equipment.

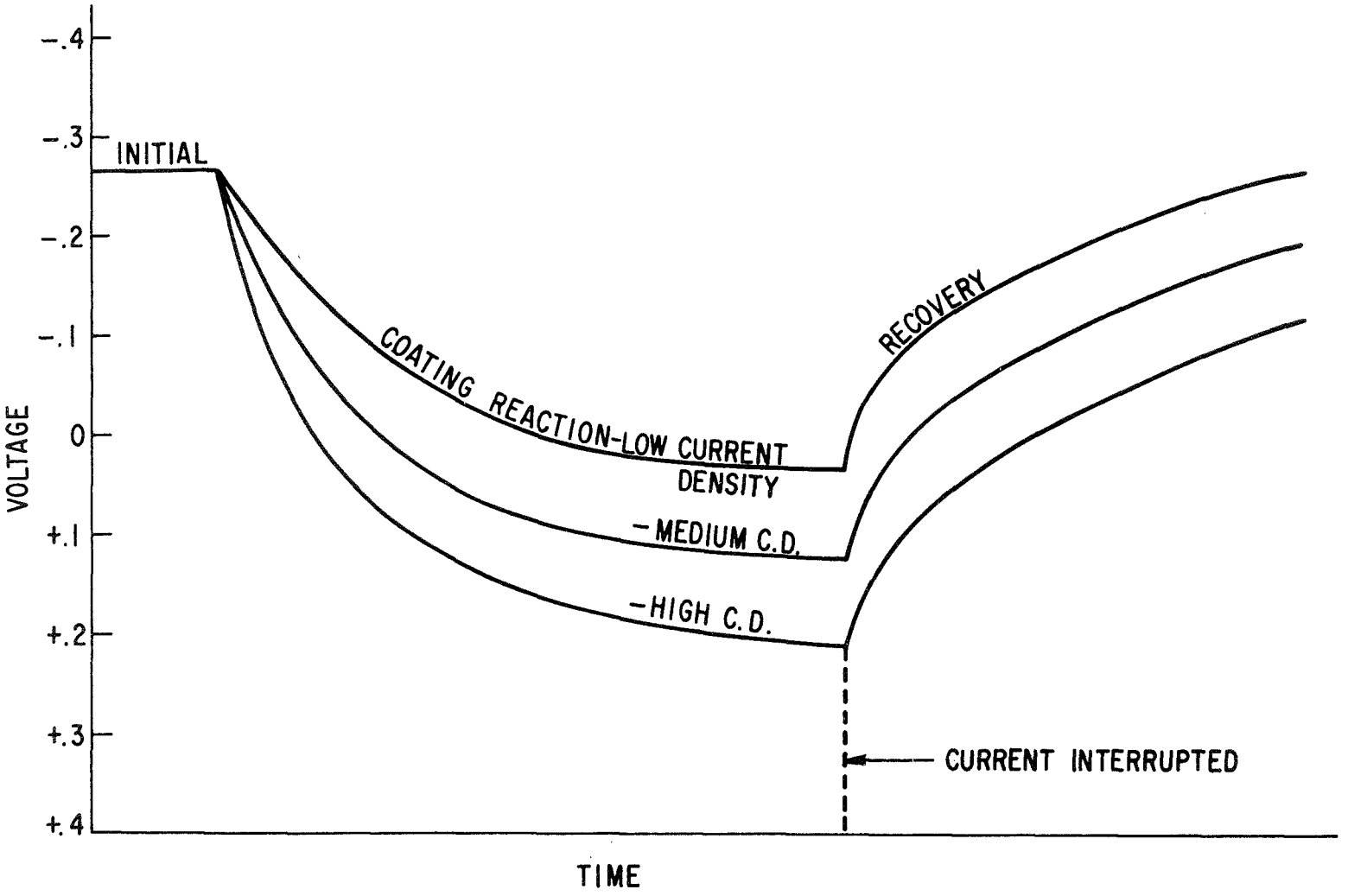

Figure 8. Typical Anode Polarity Curves for Forming Diffusion Coatings in Molten Fluorides.

of the current occurs very slowly or not at all. If cathode materials that are above the metalliding ion in the electromotive series are placed in the salt, they usually will go into solution until there is no more metalliding ion to displace. In some cases, however, the material displaced will plate on an alloy with the reacting surface, thereby lowering its electromotive activity and stopping the displacement reaction. Some success has been obtained therefore in coating metals more reactive than the metalliding agent by applying a large voltage as the sample is immersed. This procedure was employed in chromiding of the present chromium alloy. The bulk EMF of the alloy is lower than that of chromium and should thus pose no problem with displacement. However, it was felt that since the difference between the pure-chromium anode and the chromium-alloy cathode is not great, local EMF changes in the vicinity of yttrium-rich or of tantalum-rich areas of the cathode might initiate displacement reactions unless this precaution were taken.

Molten fluorides of the alkali metals and alkaline earths are used exclusively as solvents in metalliding. Their three major characteristics:

(1) Fluxing action

(2) High boiling point

(3) High stability make them uniquely suited for this purpose.

Among their important functions are:

(1) Retention of the metalliding ion in solution

(2) Dissolution of oxide films from cathode surfaces

(3) Maintenance of a low vapor pressure at operation temperature

(4) Further resistance of displacement reactions by the anode metal by virtue of the high activity of their cations

(5) Provision of a noncorrosive electrolyte

(6) Contribution of a high surface-tension medium in order to minimize salt removal by the coated parts

Choice of the specific fluoride solvent depends largely upon the temperature range to be used in metalliding. Low melting eutectic mixtures such as the Li, Na, K fluoride eutectic that melts at 850°F are generally used at lower temperatures, and higher-melting eutectics or single compounds such as LiF that melts at 1555°F are used as the metalliding temperature is increased.

Chromium is high enough in the electromotive series to form diffusion coatings on most metals. The preferred operating temperature range for chromiding is 1830-2100°F, but chromium has considerable sensitivity to oxygen impurities. Previous work on chromiding steel in fluoride salts

indicated that dendrite formation and heavy salt encrustations on the pieces made it doubtful if the process could be operated economically. However, these results were found when the salts were not clean and the process improperly operated. When the salts are substantially free of oxygen and other interfering impurities, and the rate of deposition does not exceed the rate of diffusion, smooth, dendrite-free coatings are consistently produced. It is possible to make 0.5-mil coatings in 2-1/2 minutes, 2-mil coatings in 13 minutes, and 4-mil coatings in 40 minutes at 2065°F on low carbon steels. The coatings normally have 30-35% chromium on the surface, which gradually reduces to 12% at the diffusion boundary and then breaks off sharply. The coatings are ductile, pinhole free, and very oxidation resistant.

Considerable background has been gathered in alloying chromium into the surfaces of various other substrate metals and alloys by electrodeposition from molten salt baths. Some of this work has been performed in baths of the eutectic mixture, 66.67 mole % NaF-33.33 mole % CaF_2, and other work has been done in pure LiF, each bath containing a small amount of the active salt CrF_3. Initially, the chromide coatings formed in both salt baths appeared to be identical. However, when refined analytical techniques were applied, those chromide coatings made in LiF baths were found to contain small amounts of lithium. In a separate work[22], it was found that chromium could be lithided in a LiF bath to form coatings containing up to about 0.5 atomic % Li. These coatings produced beneficial effects upon air oxidation of the samples[21] as discussed in the introductory section of this report.

Based on these findings, all of the metalliding in the present work was conducted in LiF baths. For chromiding, high-purity chromium anodes were produced by extruding and subsequent swaging of steel-jacketed iodide chromium crystals, and a small concentration of CrF_3 was added to the fused salt. Lithiding was performed with shielded carbon anodes in pure LiF.

After metalliding, any encrusted salt was removed by first converting the insoluble fluorides to water-soluble chlorides by immersion in a eutectic alkali metal chloride (LiCl-NaCl-KCl) bath followed by thorough rinsing in hot water. In the initial stages of the work, this chloride cleansing bath was yttrium gettered, but this practice was discontinued for reasons to be described in a following section.

4.1.2 Plasma Spraying

The plasma torch, a gas-stabilized, electric-arc device, was used in depositing powdered mixtures of chromium and Y_2O_3. Argon (at flow rates from 80 to 150 cubic feet per hour) was used as the primary plasma-forming gas and hydrogen (at flows of 4 to 25 cubic feet per hour) as the mixing or secondary gas. The pressurized gases, independently metered, flow into a plenum chamber where they are ionized by an arc formed between a thoriated tungsten cathode and a water-cooled copper nozzle that serves as the anode. Currents of 500 to 600 amperes were employed in this work, at potential differences of 30 to 50 volts across the electrode gap.

As the ionized gas flows into the reduced section of the nozzle, the powdered material to be sprayed is fed into the plasma through a part in the nozzle and its housing, using argon at 50 to 40 cubic feet per hour as the carrier gas. In the constricted nozzle section, the ionized gases become highly concentrated, resulting in a corresponding increase in temperature. There is also a thermal pinch effect, which tends to concentrate the current in the central region of the plasma, and self-induced magnetic fields that further constrict the plasma and result in localized temperature well in excess of 15,000°F. The powdered solids are rapidly heated to the plastic state and are propelled at high velocity onto the surface being coated, which in this work was maintained at a distance of about 5 inches from the nozzle outlet of the plasma gun.

Size ranges and chemical analysis of the Cr and Y_2O_3 powders used are shown in Table I. The powders were mixed in a twin-shell blender and were delivered to the plasma gun suspended in a flow of argon as the carrier gas, by means of a powder feed unit. This unit consists of an argon-pressurized canister mounted on a vibratory bar and equipped with a variable speed metering screw controlled by a DC drive mechanism that permits any desired powder feed rate in the range from 0 to 24 pounds per hour. The vibrator causes the powder-gas mixture to be "fluidized", thereby insuring that the metering screw is completely filled with material at all times. A safety switch is provided to prevent operation if the flow of carrier gas is interrupted. The metering screw is calibrated to a repeatable accuracy of ± 1 gram per minute at its maximum feed rate, which corresponds to its top drive speed of 400 rpm. Powdered mixtures of Cr plus 10, 30, and 50 volume percent Y_2O_3 were deposited at thicknesses of 2 to 7 mils on the Cr-7Mo-2Ta-0.1C-0.13(Y + La) substrate alloy. Steps employed in the evaluation of the various plasma-sprayed and metallided-coating variations are described in the following sections.

4.2 TESTING TECHNIQUES

4.2.1 Specimen Preparation

The substrate alloy was received from NASA in the form of 160 as-rolled 1 x 2-inch coupons with thicknesses varying from 0.063 to 0.066 inch. Each of these coupons was further sectioned by abrasive sawing into two longitudinal coupons with nominal dimensions of 0.5 x 1.5 inches and one transverse 0.5 x 1-inch section. The latter specimens were used in establishing acceptable coating techniques, and the longitudinal samples were retained for bend-test evaluation. Following this operation, all edges were rounded to a radius of approximately half the sheet thickness by hand grinding and buffing. Each sample was then electropolished at a current density of 0.2 amp/cm^2 using an electrolyte of 10% perchloric- 90% acetic acid maintained at or below 50°F. Electropolishing was used to provide a uniform starting surface and to aid in the detection of any edge cracking by fluorescent penetrant inspection. After this conditioning sequence, the samples were stress-relieved by heat treating in vacuum of 10^{-4} torr for 1 hour at 2000°F.

Table I. Characterization of Powders Used in Plasma Spraying.

Powder Type	Size, (Microns)		Major Impurities (Wt. %)				
	Range	Average	O	Fe	Mg	Ca	RE*
Coarse Cr	44 - 105	85	0.07	0.015	---	0.010	---
Fine Cr	1.6 - 10	4.5	0.40	0.2	0.15	---	---
Coarse Y_2O_3	44 - 74	62	---	0.01	---	---	0.10
Fine Y_2O_3	12 - 24	20	---	0.03	---	---	0.10

* Total rare-earth element content present as oxides.

Following the final coating step, described in the preceding sections, the samples were again vacuum heat treated under identical conditions both to provide relief of stresses that may have developed in any of the coating cycles and to enhance bonding between the coating and the substrate.

4.2.2 Oxidation Exposures

All air-oxidation exposures were conducted in resistance-heated box furnaces at 2100°F using ZrO_2 crucibles upon which lids were placed immediately after removal from the furnace to retain any spalled particles. No air circulation, other than the natural convection currents within each furnace, was imposed. All characterization of the air-oxidation behavior of the noncoated substrate alloy and of the first series of plasma-sprayed coatings was conducted prior to any oxidation of metallided coatings, since earlier data had suggested that even trace amounts of Li that might remain in the furnace after oxidation of the Li-containing metallided layers could influence the scaling rate of Li-free chromium. Most of the oxidation work in the initial stages of the program involved continuous exposures that were terminated after 50 to 200 hours at temperature. Later in the program, cyclic oxidation was also performed, in which specimens were removed from the furnace and cooled to room temperature at specified intervals during the exposure. All samples were weighed to the nearest 0.1 milligram and examined for any evidence of spalling or blistering at intervals during cyclic testing and at the termination of each exposure. At the beginning of the work, dimensional changes were also measured with a vernier micrometer, but this practice was discontinued when it was shown that the apparent thickness changes were on the order of 0.1 mil, which is no greater than the measuring error of the instrument.

Prior to the air oxidation tests, many of the specimens were pretreated in pure oxygen at 1800 to 2000°F for 1 to 4 hours. These preoxidation runs were made in a small, resistance-heated Leco furnace at an oxygen pressure of 800 torr, using ZrO_2 crucibles to support the chromium samples. Weight changes were recorded as described above.

4.2.3 Metallographic and Chemical Analysis

Standard techniques for preparation and examination of metallographic samples were employed. In most cases, specimens were sectioned and polished normal to the coated surface in the longitudinal direction of the rolled sheet. In a few instances, sectioning was performed at an angle of 7.2 degrees, to the coated surface, such that an additional taper magnification of 8:1 was imposed upon the optical magnifications selected for examination. Initial polishing was performed on Emery papers through 600 grit, with final polishing on a vibratory Syntron using a 10% chromic acid - Linde B alumina slurry as the abrasive. Specimens were first examined in the unetched condition to measure any porosity. Unless otherwise noted, all etching was performed electrolytically at a current density 2 to 3 amp/cm^2 in the following mixed reagents:

H_2O	100 ml, distilled
KOH	50 ml, 10% sol.
H_3PO_4	40 ml, 85% sol.
$K_3Fe(CN)_6$	50 ml, 10% sol.
$H_2C_2O_4$	20 g
$K_4Fe(CN)_6 0.3H_2O$	5 g

Microhardness measurements of the various types and/or layers of the coatings and substrate were made on a Kentron machine using a symmetrical diamond pyramid indenter and loads ranging from 25 to 100 grams. Hardness traverses after air oxidation were made at depth increments of 0.5 to 1 mil using a 50-gram load.

Wet chemical, x-ray fluoresence, and spectrographic procedures were employed in analysis of metallic constituents, and vacuum fusion for gas analysis. In the latter, a platinum bath at 3630°F was used, with the ratio of the weight of Pt to the cumulative weight of samples maintained above 20:1. Debye-Scherrer x-ray diffraction patterns of powdered oxidation products were used to monitor any changes in the oxide or nitride scale(s).

4.2.4 Mechanical Testing

Bend testing was exclusively used to determine the ductile-brittle transition temperature (DBTT) as affected by coating variables and air oxidation. Three-point bending was performed in an Instron frame, using an anvil with an included angle of 75 degrees, and a 0.75-inch span. The thickness (t) of the specimens varied from 0.063 to 0.080 inch, depending on the type and thickness of the coating, and a ram with a radius (R) of 0.250 inch was used in each case. Use of this radius imposed tensile strains ranging between about 11 and 14% on the convex surfaces. Most tests were made at a head speed of 1 ipm, with a few being conducted at 0.05 ipm to provide comparison to earlier data.

The DBTT for each coating-exposure condition was defined as the average of the lowest temperature at which a full 105-degree bend was obtained and the highest temperature at which failure occurred at any lower bend angle. With rare exceptions, these two values differed by no more than 50°F. Tests in latter stages of the work were all made to full bend or failure. In the screening phases of the work, a multiple-bend technique (in which a single specimen was bent through predetermined angles at successively lower test temperatures) was used to provide an early assessment of the protectiveness of the coatings. In each case, the first appearance of a crack that caused a sudden drop in load on the chart recorder of the testing machine was interpreted as failure. These cracks usually propagated across the specimen immediately; but, occasionally, at test temperatures of 800°F or above, a crack was arrested near the neutral axis of the specimen.

4.3 OVERALL PROGRAM PLAN

The first stages of the program were devoted to characterizing the DBTT of the substrate alloy and to establishing suitable processing sequences for producing coatings of the following three types:

1. Chromided layers from LiF-CrF_3 bath, pure Cr anode

2. Lithided layers from LiF bath, shielded C anode

3. Plasma-sprayed Cr + Y_2O_3 layers

Coatings of these types, covering relatively wide ranges of application parameters, were evaluated with respect to thickness, uniformity, density, microstructure, and microhardness on 1/2 x 1-inch samples of the substrate alloy. Once limits for satisfactory coatings were thus determined, bend-test samples were prepared from each of the three systems near mid-point conditions and tested in the following states:

A. As coated

B. (A) plus vacuum annealed 2 hours/2000°F

C. (A) plus preoxidized 2 hours/2000°F in pure O_2

D. (C) plus 2100°F/200 hours/argon

Further screening of the coatings was performed on duplicate bend coupons of several selected modifications of each coating type by preoxidizing for short times (1 to 4 hours) at 1800 to 2100°F in pure oxygen; these screenings were followed, in the case of those coatings that resulted in adherent scales, by 50-hour continuous air oxidation at 2100°F. Weight changes were measured after each exposure. Effects of the 50-hour air exposure on the DBTT were approximated by using a multiple-bend plus full-bend technique in which the first sample was bent through an angle of 15 degrees at 1000°F, then through additional angles of 15 degrees at successively lower temperatures in decrements of 100°F until failure occurred. The second sample was then deformed to a 45-degree bend or failure at a temperature 100°F above the value determined as described above, then to a full 105-degree bend or failure at 50°F above the failure temperature of the initial specimen. Following bend testing, microstructural examination and microhardness testing were performed as outlined in Section 4.2.3.

Coating variations of each type that exhibited the greatest ductility retention in 50-hour screening tests were applied to a second series of bend specimens. These were vacuum annealed and preoxidized as described above and then subjected to continuous 100-air exposures at 2100°F. Those coatings that were adherent and exhibited relatively small weight gains

under these conditions were then further exposed for 100 hours at 2100°F under cyclic conditions, in which specimens were cooled to room temperature at 2-hour intervals for the first 20 hours and at 20-hour intervals thereafter. Samples from this group were bend tested and examined metallographically as described above.

Based on the results obtained to this point, the most attractive modifications of each individual coating type were selected for evaluation as combined coating systems. In each case, the first coating applied was the most effective of the chromided layers. This enabled the isolation of reactive constituents of the substrate alloy from the air environment in case outer layer(s) of the coating were penetrated or otherwise became inoperative. Over this chromided undercoat were applied selected lithided plus plasma-sprayed Cr-Y_2O_3 layers, and plasma-sprayed Cr-Y_2O_3 layers alone. These multiple-component coatings were tested in the same manner as that described above for the individual systems - short exposures in pure oxygen followed by 50- and 100-hour exposures in air at 2100°F, the latter both continuous and cyclic. Evaluation consisted of measurement of weight change, observation of the adherence of the scale, approximation of the DBTT by the multiple-bend technique, metallographic examination, and microhardness testing.

Finally, based on the data gathered in the screening and preliminary-evaluation stages of the work, the four most attractive coatings were selected and subjected to more critical test conditions. Air-oxidation exposures were extended to 200 hours using continuous and cyclic exposures; coated specimens were tested with intentional defects, in addition to testing in the as-coated condition; and, the rate of cooling to room temperature during cyclic oxidation was varied. Oxidation products were identified by x-ray diffraction analysis, and the oxygen and nitrogen contents of the substrate were determined by the vacuum-fusion technique after removal of the scale and coating by grinding.

5.0 EXPERIMENTAL RESULTS

5.1 SUBSTRATE CHARACTERIZATION

The alloy used for the substrate in this work was developed in a separate NASA program undertaken by this laboratory[14], and was procured by NASA as mill product, the production of which has been described in detail by Slaughter et al[27]. A chemical analysis of the heat used here is shown in Table II. The average as-received hardness of 335 kg/mm^2 was reduced to 320 ± 15 kg/mm^2 by a 200-hour anneal in vacuum at 2100°F.

Results of weight gain measurements in 100- and 200-hour cyclic air-oxidation tests on the alloy at 2100°F are shown in Figure 9. The 200-hour data plotted are average values from four specimens, and results for the first 100 hours are averages of eight specimens. Individual measurements were rather uniform, with terminal weight gains of 5.3 to 6.2 mg/cm^2 at the end of 200 hours exposure. Some spalling occurred in each sample, in contrast to the behavior in continuous 200-hour oxidation exposure where weight gains of 4.9 to 5.5 mg/cm^2 were recorded. The scales were adherent after the single cooling cycle to room temperature. Intergranular nitridation accompanied by subsurface hardening was observed to depths of 15 to 18 mils in the cyclic-oxidation samples as shown by the photomicrograph and hardness traverse in Figures 10 and 11, compared to about 10 mils after continuous 200-hour oxidation. Note in Figure 10B that, although the scale on the continuously-exposed sample is adherent, there is considerable blistering of the oxide which probably accounts for the observed nitride formation. The predominant nitride phase was identified by x-ray diffraction as Cr_2N, with a hexagonal unit cell a = 4.782Å, c = 4.446Å. There were also trace amounts of another phase in the extract that could be indexed as hexagonal a = 5.182Å, c = 2.914Å. These unit cell values are close to those for TaN, and suggest that some TaN has formed in intergranular regions.

Measurements of the DBTT of the alloy were made after stress relieving for 1 hour at 2000°F in vacuum, after vacuum annealing for 200 hours at 2100°F, and after both continuous and cyclic air oxidation for 200 hours at 2100°F. Results of the bend tests are presented in Table III. The 200-hour vacuum anneal at 2100°F, which results in complete recrystallization and some agglomeration of the TaC dispersion, yields a DBTT of about 580°F, only a moderate increase over the value of 490°F measured in the stress-relieved condition. It should be noted in passing, that the as-received sheet was in fact partially recrystallized during the processing sequence employed by the producer, and that the yield strengths recorded in Table III are consequently much lower than those measured earlier on warm-worked bar stock of the same alloy[14].

Air oxidation, as expected, causes a drastic increase in the DBTT. After either continuous or cyclic exposure at 2100°F, bends of less than 15 degrees were measured at all test temperatures through 1400°F, which

Table II. Chemical Analysis of Substrate Alloy.

Element	Average Concentration (Wt. %)	
	Heat 131	Heat 140
Cr	Balance	Balance
Mo	7.01	7.12
Ta	2.10	2.14
C	0.099	0.103
Y	0.09	0.17
La	0.04	0.12
O	0.0049	0.0030
N	0.0032	0.0037
H	0.0016	0.0030
S	< 0.002	< 0.002
P	< 0.001	< 0.001
Al	0.007	0.002
Fe	0.003	0.003
Hf	< 0.05	< 0.05
Cb	< 0.03	< 0.03
Ni	< 0.001	< 0.001
Si	0.02	0.01
Ti	0.001	< 0.001
V	< 0.001	< 0.001
W	< 0.05	< 0.05
Zr	0.0050	0.0070

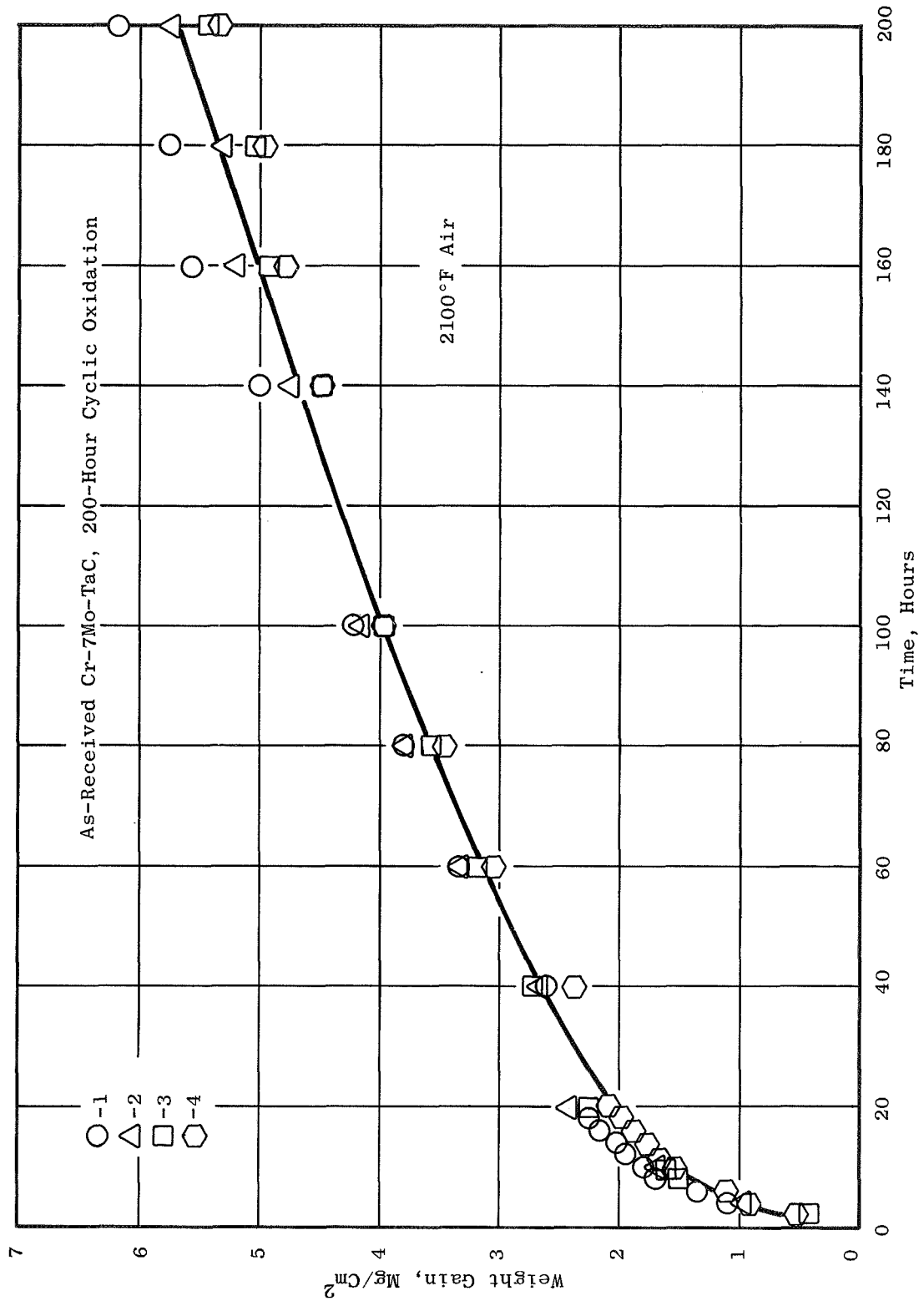

Figure 9. Air Oxidation of Substrate Alloy.

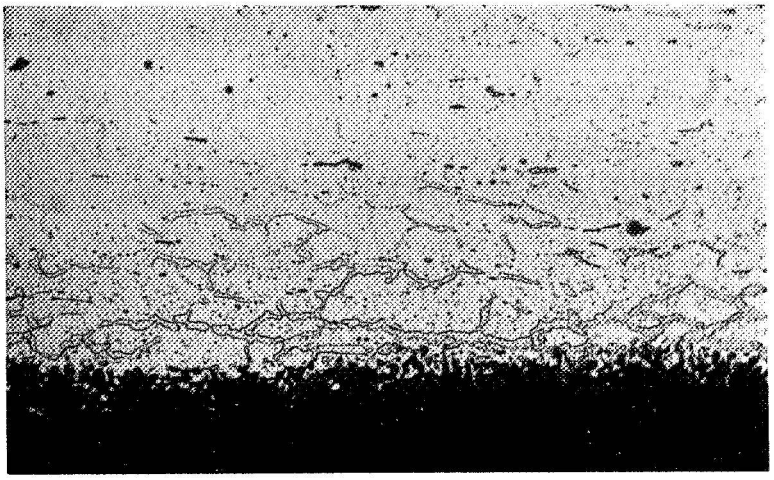

A. Cyclic Exposure Mt. A7886

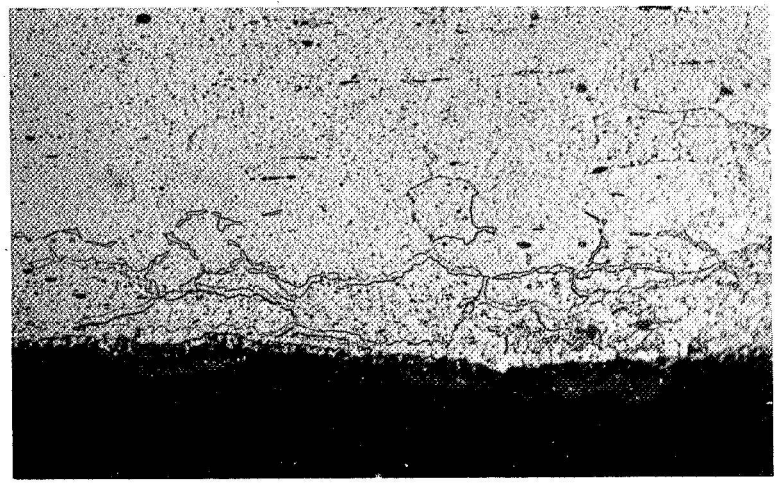

B. Isothermal Exposure Mt. A8573

Figure 10. Surface Microstructure of Cr-7Mo-TaC Alloy after 200-Hour Air Oxidation at 2100°F (500X).

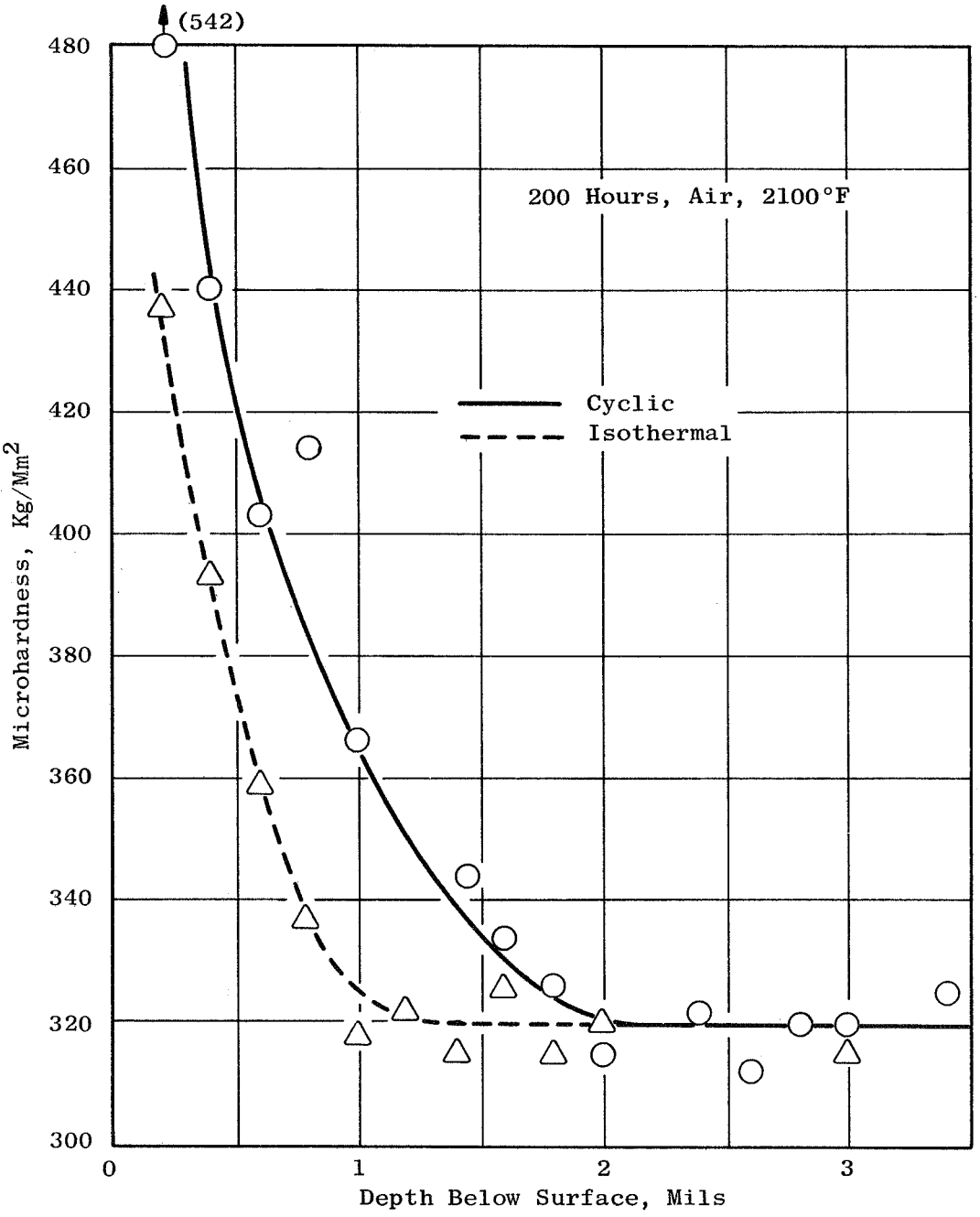

Figure 11. Effect of Air Oxidation on the Subsurface Hardening of Cr-7Mo-TaC.

Table III. Bend Properties of Cr-7Mo-2Ta-0.1C-0.13(Y+La) Alloy.

	Test Temp (°F)	Bend Angle (°)	Fiber Stress At Yield (KSI)	DBTT* (°F)
A. Stress Relieved 2000°F/1 Hr/Vac	400	8	82.5	
	450	35	62.5	
	475	54	47.6	490
	500	Full	49.6	
	600	Full	51.7	
B. Annealed 2100°F/200 Hrs/Vac	400	2	12.4F	
	500	25	53.7	
	550	32	60.3	480
	575	90	53.4	
	600	Full	50.4	
C. Oxidized 2100°F/200 Hrs/Air (Isothermal)	600	0	37.2F	
	1000	3	26.1	>1400
	1200	4	39.2	
	1400	6	47.1	
D. Oxidized 2100°F/200 Hrs/Air (Cyclic)	800	4	54.8	
	1000	7	47.5	
	1200	12	41.5	>1400
	1400	14	41.9	

* Approximate temperature for full 105° bend of 0.063-inch sheet samples over radius of 4t.

(because of distortion of the V-block and ram at higher temperatures) is near the upper limit of the test method. It is of interest that some plastic deformation preceded fracture at test temperatures as low as 800°F; and, that at a given test temperature, somewhat greater deformation was observed after cyclic than after continuous air exposure. In view of the greater depth of nitride formation in cyclic oxidation, this behavior at first appears anomalous. It is probably associated with the heavier layers of adherent oxide on continuously-exposed samples. The strain required to initiate cracks in the scale decreases as the scale thickness increases; and, once these cracks are formed, they cannot be arrested by the nitrogen-embrittled matrix alloy. On the other hand, it has been shown[28] that the oxide scale is not directly responsible for the large increase in the DBTT, since exposures of carbide-strengthened Cr-Y alloys in pure oxygen result in increases in the DBTT of only 100 to 200°F at the most. In the absence of nitridation, plastic bending of such samples at intermediate temperatures results in profuse cracking of the oxide, but the cracks do not propagate into the matrix. Further work along the same lines was performed in this study on coatings that were pretreated in pure oxygen, the results of which also indicate that oxide formation, per se, has little adverse effect on the DBTT as will be shown in the following sections.

5.2 DEPOSITION AND OXIDATION OF CHROMIDED COATINGS

Samples of the substrate alloy were chromided in a molten $LiF-CrF_3$ bath at temperatures from 1800 to 2100°F for periods of 30 minutes to 4 hours over a range of current densities. Under the conditions examined, weight gains from about 3 to 25 mg/cm^2 were recorded, corresponding to thicknesses of chromium ranging from less than 0.2 to about 1.4 mils. Regardless of thickness, the diamond pyramid microhardness of the chromided layers was 125 ± 5 kg/mm^2 at a 50-gram load. Deposition parameters covering the ranges investigated in this work are shown in Table IV.

Since there is only a small difference between the EMF of chromium and that of the chromium-base alloy being coated, the coulombic efficiencies obtained in the chromiding work were consistently lower than 100% of theoretical. These efficiencies were calculated from the weight gains measured after removal of the encrusted salt by the cleaning procedure described in Section 4.1.1. Most of the metalliding conditions yielded efficiencies between 70 and 80%, but values as low as 50% and as high as 98% were measured. Note that both the high and low coulombic efficiencies were unusually associated with relatively high current densities.

At the higher current densities, there was a marked trend toward deposition and growth of the chromium as discrete particles that resemble dendritic spikes, rather than growth as a continuous surface layer. This behavior, which is illustrated in Figure 12A, was particularly pronounced under conditions that yielded weight gain rates above about 15 $mg/cm^2/hr$. Lowering the current density to 20 to 30% of the highest values employed virtually eliminated the nonuniform deposition as shown in Figure 12B. Isolated examples of accelerated growth were very rarely observed at low current density and, when present, were confined to end faces of the specimens near the electrical contacts.

Table IV. Deposition Parameters Employed in Chromiding.

Designation	Temp (°F)	Time (Min)	Relative Current Density	Wt Gain (mg/cm^2)	Efficiency (%)
A1*	1905	60	3.3	10.3	69.0
A2*	1905	60	3.3	-	52.5
B*	1830	120	4.3	14.8	59.8
C*	2010	30	2.7	4.7	79.8
D*	1940	180	1.4	13.3	73.7
E1	1960	180	1.4	14.1	79.2
E2	1960	180	1.3	13.4	76.0
E3	1960	180	1.4	13.8	76.2
E4	1960	180	1.35	14.7	82.4
F	1940	120	1.0	7.1	78.3
G1	1940	30	5.2	6.8	62.0
G2	1940	30	5.0	10.7	97.9
G3	1940	30	5.0	6.0	55.0
H	2010	30	3.0	5.4	77.1
I	1830	180	2.0	17.6	68.0

* Inadequately cleaned samples

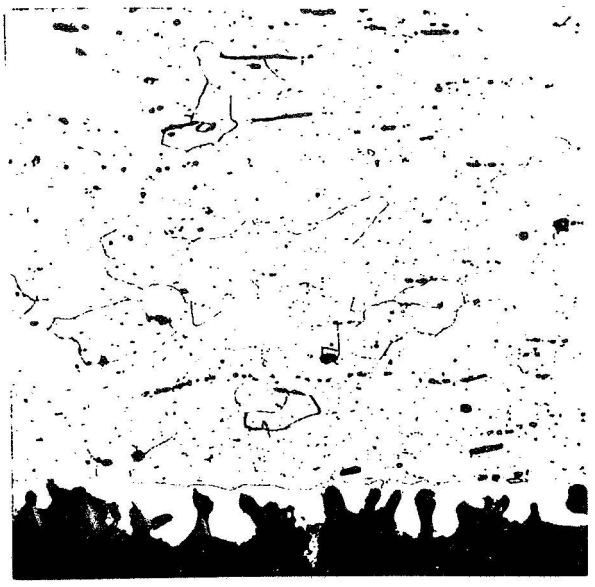

A. Relative Current Density 5.0 — Mt. A5823

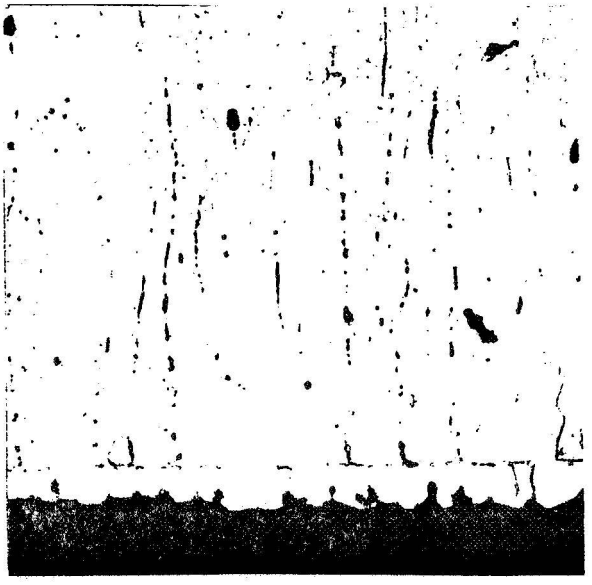

B. Relative Current Density 1.4 — Mt. A6353

Figure 12. Representative Chromided Layers Produced at 1950 ± 10°F.

Some of the initial treatments in pure oxygen were conducted on samples that had been produced at high current density and which had apparent coulombic efficiencies above 90% of theoretical. High weight gains were measured and gross spalling of the oxide occurred upon cooling these specimens to room temperature after a 2-hour exposure in oxygen at 2000°F. Spectrographic analysis of the spalled scale indicated a high yttrium content. Since the chromided coatings were still intact, only the oxides having spalled, there appeared to be no possibility that the Y in the oxide could have come from the matrix alloy. The only other known source of Y was the chloride cleansing bath, in which a Y-gettered LiCl-NaCl-KCl eutectic melt was employed to convert insoluble fluoride salts to soluble chlorides. Apparently, some Y in an insoluble form was being transferred to the specimen surfaces during the cleaning process and was entrapped in the cavities between the dendritic-like spikes that resulted from chromiding at high current density. The more-uniform chromided layers produced at low current density did not form spalling oxides upon pretreatment in pure oxygen after cleaning in Y-gettered chlorides, but did show very high weight gains and gross spalling during subsequent air oxidation under the screening conditions of 50 hours at 2100°F.

Moderate concentrations of Y in chromium alloys are, of course, beneficial to oxidation behavior. Yttrium is extremely reactive, and its concentration at the surface (particularly in the form of a complex compound with either the alkali metals or the halogens) could be the cause of the accelerated oxidation kinetics and nonadherent scales. To further isolate the source and contribution of Y, a second series of chromided samples was prepared and cleaned by immersion in a Y-free chloride melt, followed by water rinsing and 1-hour vacuum annealing at 2000°F. None of these samples exhibited accelerated reaction or spalling oxides after a 2-hour exposure in oxygen at 2000°F or 50-hour air oxidation at 2100°F, and no Y was detected in spectographic analysis of the scales. Consequently, all further cleaning of metallided samples was performed in Y-free chloride baths.

Measurements of the oxidation behavior of chromided coatings are summarized in Table V. Included for comparison are some of the data obtained from the inadequately-cleaned samples described above. The best behavior was observed in specimens chromided at low current densities for 2 to 3 hours at 1940 ± 20°F. Quite low weight gains were measured after 50- and 100-hour air exposures at 2100°F and only slight spalling occurred under the cyclic exposure conditions. Weight change data for the best chromided coatings in air oxidation at 2100°F are compared to those for high-purity iodide chromium and the uncoated Cr-7Mo-2Ta-0.1C-0.13(Y + La) alloy in the log-log plot of Figure 13. The kinetics in each case are very nearly parabolic, at least for the first 50 or 60 hours of exposure. After that period (which corresponds to the onset of slight spalling in the chromided specimens upon cyclic cooling to room temperature) the oxidation rate becomes faster, and the reaction appears to approach linear kinetics.

Table V. Oxidation Behavior of Chromided Samples.

	Chromiding Conditions			Oxidation Weight Gain (mg/cm^2)			
	Temp	Time	Rel	2000°F O_2	Isothermal		Cyclic
Desig	(°F)	(Min)	C.D.	2 Hrs	50 Hrs	100 Hrs	100 Hrs
A1*	1905	60	3.3	2.2AS	2.46S	-	-
B*	1830	120	4.3	5.3S	2.73S	-	-
C*	2010	30	2.7	0.8A	5.29S	-	-
D*	1940	180	1.4	1.3A	7.73S	-	-
E1	1960	180	1.4	1.4A	0.71A	1.04A	1.32A
E4	1960	180	1.4	1.6A	0.68A	1.10A	1.17A
F	1940	120	1.0	2.0A	0.82A	0.98A	1.22AS
G2	1940	30	5.0	2.6B	5.81A	8.40S	-
H	2010	30	3.0	1.9A	2.61A	3.70A	4.05B
I	1830	180	2.0	1.7A	1.85A	2.62A	2.98B

* Inadequately cleaned samples

A = Adherent oxide

S = Spalling oxide

B = Blistered oxide

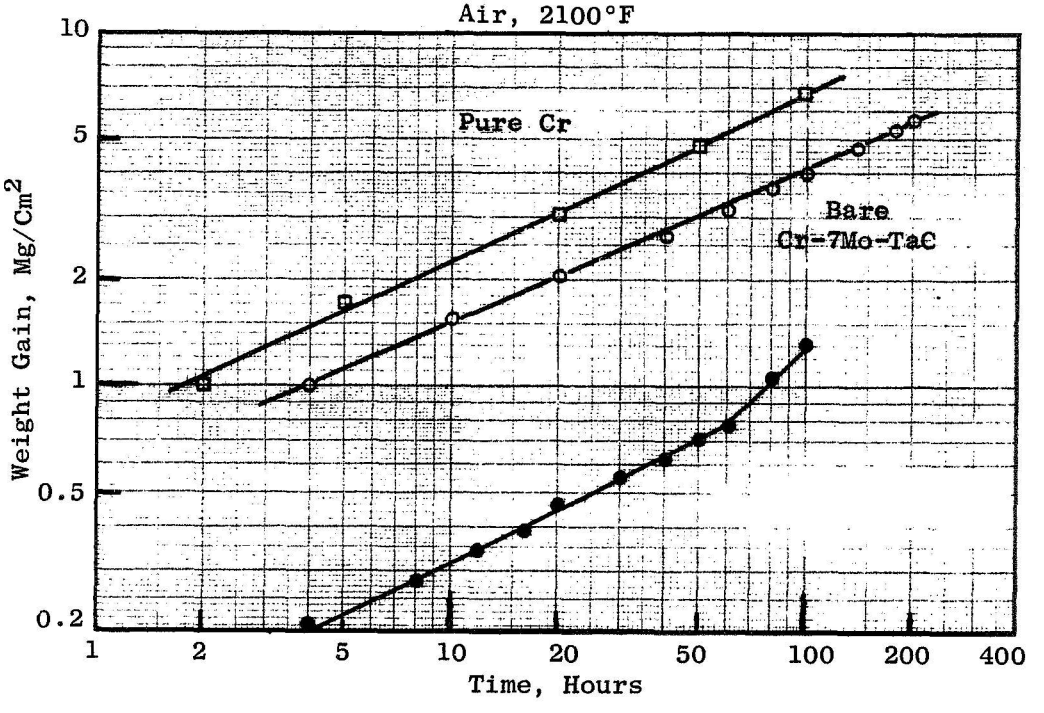

Figure 13. Air Oxidation of Chromided (E1) Alloy at 2100°F.

However, during the period in which the air oxidation rates are parabolic, the rate constant for the chromided coating is lower than that of high-purity chromium by well over an order of magnitude.

It was pointed out earlier that Cook has shown that chromiding in a $LiF-CrF_3$ bath results in the transference of trace amounts of Li in addition to Cr. In the present work, analyses of the chromided deposits by wet chemical, x-ray fluorescence, and spectrographic techniques failed to detect Li or any other metallic impurities at levels above those present in the high-purity iodide chromium anode. Facilities for activated neutron analysis, which Cook had used to confirm the presence of Li, were not available within the time and funding limits of this study and were thus not employed. Nevertheless, the large decrease in the oxidation rate of the uniform chromided layers compared to that of pure chromium provides an indication that some Li has been codeposited, since none of the other trace impurities could account for the observed improvement. In fact, as demonstrated by Hagel[1], impurities increase rather than decrease the oxidation rate of iodide chromium.

Photomicrographs of the most effective chromided coating (Condition E in Table V) after continuous and cyclic air oxidation for 100 hours at 2100°F are shown in Figure 14. In each case, there is some blistering of the scale, and spalling was noted after 60 hours of cyclic exposure. Although no nitride layers have formed in either case, and the hardness of the substrate alloy remained at its pre-exposure value of about 320 kg/mm^2, there is hardening of the chromided layer below the scale from its virgin value of 125 kg/mm^2 to about 180 kg/mm^2 and 220 kg/mm^2 after continuous and cyclic exposure respectively. Without a coating, 100-hour air oxidation of the substrate alloy resulted in a subsurface nitride layer with a hardness above 1000 kg/cm^2 and intergranular nitride formation to a depth of about 15 mils.

5.3 DEPOSITION AND OXIDATION OF LITHIDED COATINGS

Direct lithiding of the substrate alloy was not attempted in this work. Instead, the approach selected was to lithide after first chromiding the substrate (under conditions described in the preceding section), in order to isolate the reactive constituents of the alloy (TaC particles, Y-rich phases) from the surface that would subsequently be exposed to air.

Deposition parameters employed in lithiding, and the effects of variations in deposition time and current density on the weight changes and coulombic efficiencies, are shown in Table VI. In contrast to the behavior in chromiding, where properly-cleaned samples showed rather reproducible behavior except under the highest current density conditions, lithiding response was extremely erratic. On the basis of prior work reported by Tedmon and Hagel[20], rather low coulombic yields had been expected using the shielded carbon anode. However, in several instances in the present work, not only were the yields low, but weight losses were recorded at lower current densities. This behavior suggests the buildup

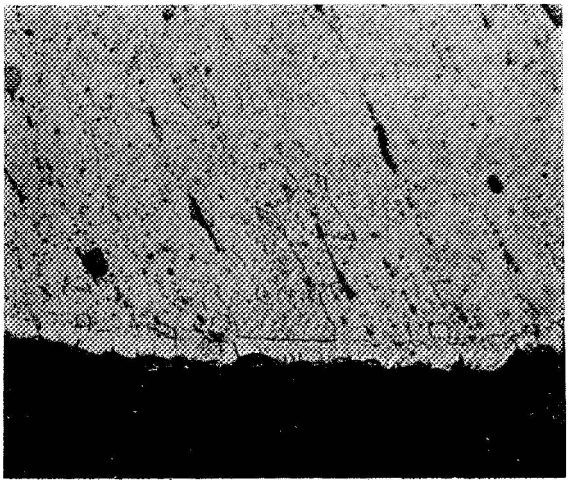

A. Cyclic Mt. A9058

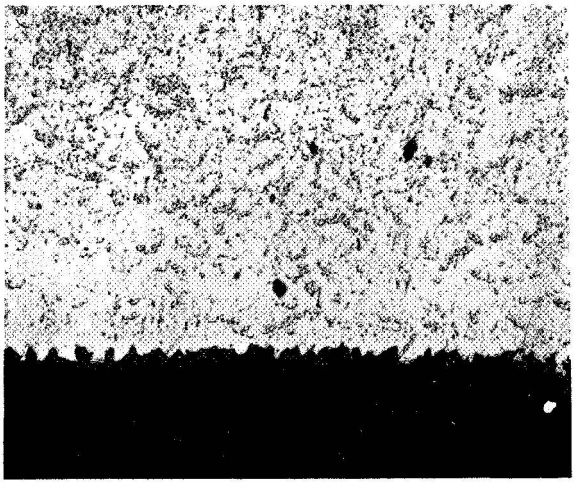

B. Isothermal Mt. 7875

Figure 14. Microstructures of Chromided (E) Surfaces after 100-Hour Air Oxidation at 2100°F (250X).

Table VI. Deposition Parameters Employed in Lithiding*.

Designation	Temp (°F)	Time (Min)	Current Dens (mg/cm^2)	Wt Gain (mg/cm^2)	Efficiency (%)
J1**	1830	60	20	-0.11	-
J2**	1830	60	20	0.04	-
J3**	1830	60	20	-0.17	-
K1**	1830	90	30	-0.12	-
K2**	1830	90	30	-0.03	-
K3**	1830	90	30	0.06	-
L1**	1830	120	20	-0.04	-
L2**	1830	120	20	0.03	-
J1	1830	60	20	0.08	-
J2	1830	60	20	0.02	-
K1	1830	90	30	0.11	-
K2	1830	90	30	0.10	-
K3	1830	90	30	0.04	-
L1	1830	120	20	0.01	-
L2	1830	120	20	0.05	-
M1	1830	90	10	0.04	-
M2	1830	90	10	0.02	-
N1	1830	90	40	0.12	-
N2	1830	90	40	0.03	-

* All samples previously chromided 3 hours at 1960°F in LiF-CrF_3 bath at relative C.D. of 1.4, Condition E in Table IV.

** Deposition runs made by immersing samples with current off. All others had current of about 45 ma/cm^2 applied before immersion.

of impurities on the cathode, which could cause local reversal of electrode polarity; but, even after repeated cleansing of the LiF bath by metalliding a nickel cathode, weight losses were still sometimes observed upon lithiding the previously-chromided substrate alloy. Even when the cell was operating in the proper direction, consecutive runs under identical deposition conditions yielded weight gains that differed rather widely, as indicated in the first portion of Table VI.

The largest absolute differences in mass transfer were noted at high current density and temperatures of 1900°F and above; and, as noted above, some runs at low current density resulted in weight losses of the cathode. In order to circumvent this problem, the practice adopted was to immerse the sample in the LiF bath at 1830°F with a rather large overvoltage applied. After immersion, the voltage was reduced to provide a lower value of current density than was maintained throughout the metalliding run. Results obtained under these dual-voltage conditions are shown in the latter portion of Table VI. Weight gains were less erratic than earlier results, in that small positive mass transfer values were invariably obtained; but, the relative differences between coulombic yields in identical runs are still much greater than those experienced in chromiding. Photomicrographs that are representative examples of the structural differences observed in lithiding are shown in Figure 15. From the cross section in Figure 15A, the average depth of Li penetration is seen to be about 0.8 mil. The weight gain in this run, which was among the highest observed, was 0.10 mg/cm^2. Assuming all the gain to be Li, these figures result in an average Li concentration of about 0.78 weight percent in the chromided layer. This is much greater than the concentration of 0.5 atomic percent (0.067 weight percent) that Tedmon and Hagel estimated from sputter-ion analysis after lithiding of pure chromium[20], but is still rather small.

Results of oxidation tests on several lithided coatings, produced by the dual-voltage technique, are summarized in Table VII, and extremes in the surface and subsurface microstructure after air oxidation are shown in Figure 16. Weight gains during short exposure to oxygen at 2000°F were significantly lower than those shown by the chromided coatings under the same conditions, but they also exhibited much more scatter, from less than 0.2 to greater than 1.0 mg/cm^2 in 2-hour exposures. The samples which had the higher gains in preoxidation exhibit rather high reaction rates, spalling oxides, and intergranular nitrogen attack upon subsequent air oxidation for 50 hours at 2100°F. Lithided samples that had weight gains below about 0.4 mg/cm^2 during preoxidation, in general, behaved well in subsequent air oxidation under isothermal conditions for 50 or 100 hours at 2100°F. However, as noted in Table VII, even these samples spalled severely under cyclic oxidation exposures.

Comparison of the oxidation data in Table VII with the lithiding deposition results shown in Table VI indicates that there is no first-order relationship between air oxidation behavior and prior lithiding history. Samples prepared under identical conditions, even when their weight gains

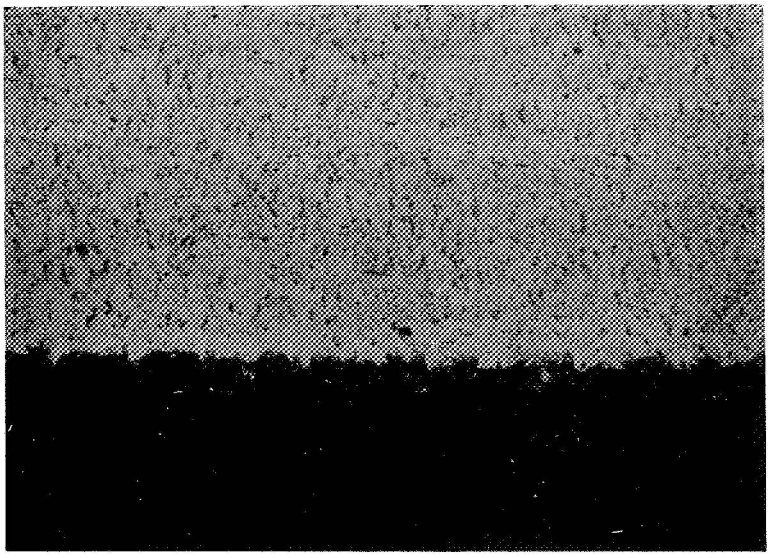

A. Condition K2 Mt. A8398

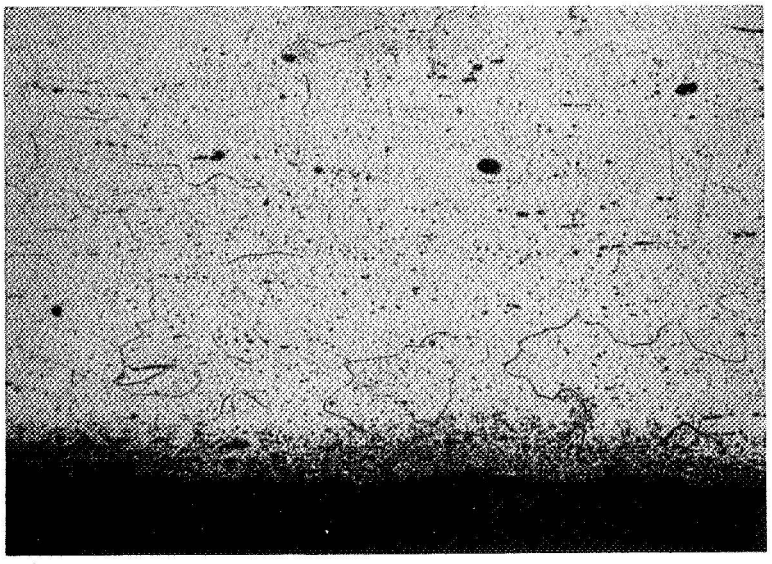

B. Condition K3 Mt. A6645

Figure 15. Representative Microstructures of Lithided Surfaces Produced at 1830°F (500X).

Table VII. Oxidation Behavior of Lithided Samples

	Lithiding Conditions*			Oxidation Weight Gain (mg/cm^2)			
	Temp	Time		2000°F O_2	Isothermal		Cyclic
Desig	(°F)	(Min)	(ma/cm^2)	2 Hrs	50 Hrs	100 Hrs	100 Hrs
J1	1830	60	20	0.3A	0.67A	4.16S	-
J2	1830	60	20	0.2A	1.22AS	-	-
J2**	1830	60	20	1.1A	3.64S	-	-
K1	1830	90	30	0.3A	0.75A	1.20A	5.82S
K2	1830	90	30	1.4A	4.06S	-	-
L1	1830	120	20	0.2A	1.09A	1.46A	6.20S
L2	1830	120	20	0.9A	3.82S	-	-
M1	1830	90	10	1.2A	2.58S	-	4.26S
N1	1830	90	40	0.5A	1.34AS	3.57S	5.40S

* See specific details and notes in Table VI

A = Adherent Oxide

S = Spalling Oxide

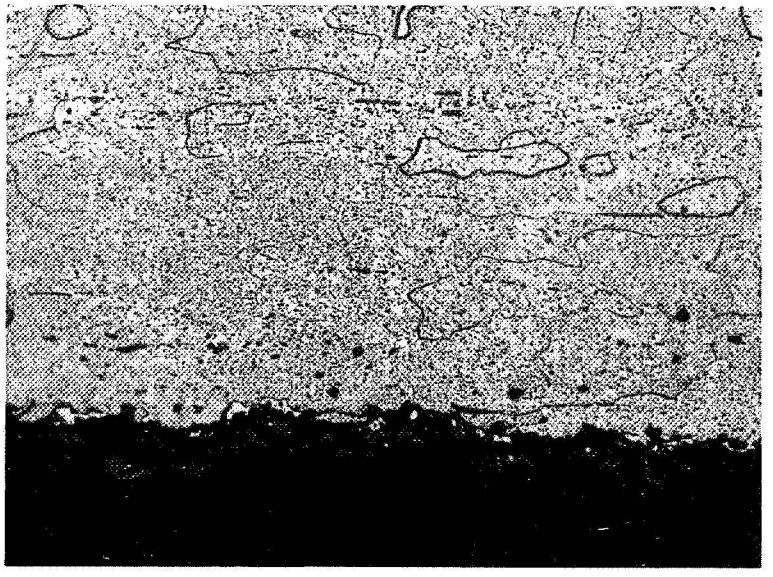

A. Condition K1 Mt. A9065

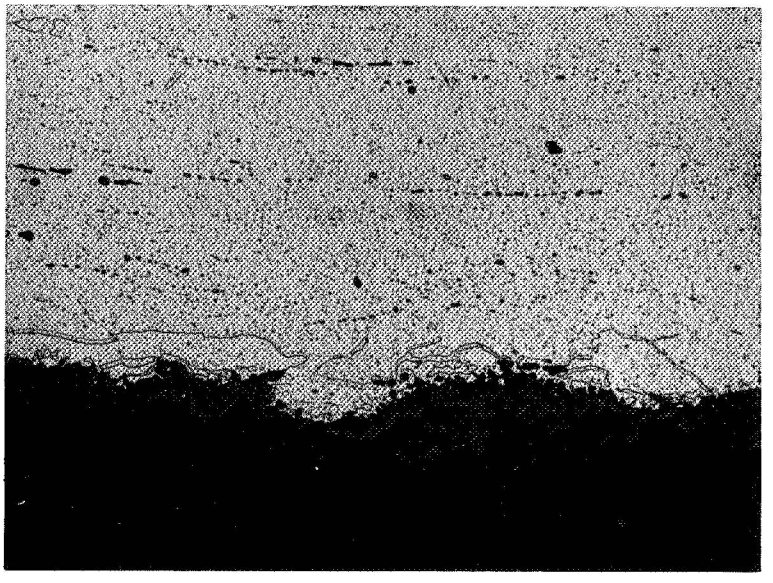

B. Condition K2 Mt. E1617

Figure 16. Effects of 50-Hour Isothermal 2100°F Air Exposure on the Microstructure of Lithided Surfaces (250X).

in lithiding were quite close, exhibited widely different oxidation behavior. Although short exposures in oxygen were relatively effective in identifying lithided samples that would behave satisfactorily in air oxidation, the air-oxidation resistance of the best lithided layers developed in this work was inferior in each instance to that of optimum chromided coatings. It would appear that, within the limits investigated in the present study, the trace amounts of lithium that are incorporated during chromiding are superior to lithiding per se. Results of bend tests of oxidized samples, to be presented in a following section, also lend support to this observation.

5.4 DEPOSITION AND OXIDATION OF Cr-Y_2O_3 COATINGS

Powdered mixtures of chromium with 10, 30, and 50 volume percent Y_2O_3 were plasma sprayed on samples of the substrate alloy using techniques described in Section 4.1.2. Most of the screening work was performed with 30% and 50% Y_2O_3 powders using powder feed rates of 8 to 12 pounds per hour. Ranges of deposition parameters investigated in this study are summarized in Table VIII, and representative microstructures are shown in Figure 17.

The initial spraying work was done with the coarser powders, the size ranges of which were shown earlier in Table I. Rather nonuniform deposition was obtained. Most of the powder particles exhibited the usual flattening from their original spheriodal shape into disk-shaped particles, with their short dimension parallel to the direction of incidence in spraying. However, as illustrated in Figure 17A, use of the coarser powders sometimes resulted in the deposition of rather large spherical particles with a high concentration of porosity in their immediate vicinity. Although none of the deposits approached full density, even after vacuum annealing at 2000 or 2200°F, measurements of the volume fraction of pores in areas remote from nonuniform particles also indicated a general tendency toward higher porosity in deposits produced from coarser powders. For these reasons, the finer powders with mean particle diameters of 4.5 microns for the Cr and 20 microns for the Y_2O_3, were used in the balance of the work.

The most-uniform and most-reproducible structures were produced using a high-velocity, low-dwell nozzle at powder feed rates of about 8 pounds per hour and at power levels of about 22 kilowatts. A typical deposit produced from finer powders under these conditions is shown in Figure 17B. Significant increases in the powder feed rate and/or the power level tended to produce nonuniform deposits and higher porosity, as shown in Figure 17C. There also appeared to be some increase in porosity as the volume fraction of Y_2O_3 was increased, as illustrated by comparison of Figures 17B and 17D. This behavior apparently results from less perfect bonding between unlike particles in the sprayed mixture, since, in general, the voids are concentrated in Cr-Y_2O_3 interfacial regions while the Y_2O_3 - Y_2O_3 (and particularly the Cr - Cr) interfaces are relatively free of porosity in the as-sprayed and annealed condition.

Table VIII. Deposition Parameters in Plasma Spraying

Sample	Nozzle	Amps	Volts	KW	Primary (Argon)	Secondary (Hydrogen)	Carrier (Argon)
3874	E	600	35	21	90	4	37
3875	E	600	40	24	90	10	37
3876	E	600	44	26.4	150	10	37
3877	Std A	600	30	18	100	0	37
3878	Std A	500	45	22.5	80	25	37
4520	Std A	500	40	20	110	1.5	20
4521	Std A	500	45	22.5	90	3	20
5729	Hi Vel	500	48	24	90	3	5
5730	Hi Vel	600	46	27.6	90	1.5	5
5731	Hi Vel	500	45	22.5	90	1.5	5

A. Coarse Powders
30% Y_2O_3
6.5 Mils
22.5 KW
Mt. A3828 (500X)

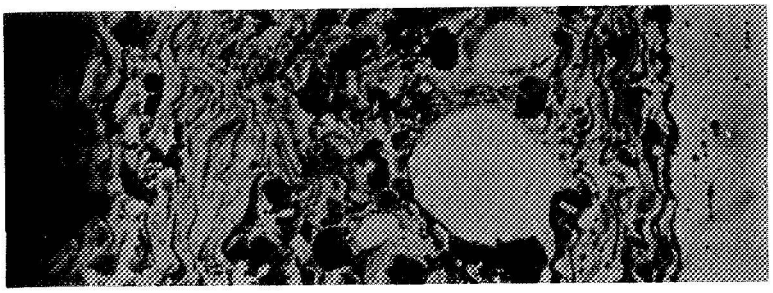

B. Fine Powders
30% Y_2O_3
4.5 Mils
22.5 KW
Mt. E1883 (250X)

C. Fine Powders
30% Y_2O_3
2.5 Mils
27.6 KW
Mt. E1865 (250X)

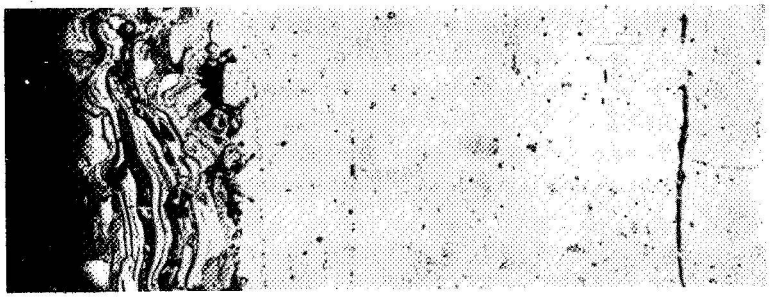

D. Fine Powders
10% Y_2O_3
4.5 Mils
22.5 KW
Mt. E1884 (250X)

Figure 17. Microstructures of Plasma-Sprayed Cr + Y_2O_3 Coatings.

Effects of screening oxidation exposures on weight changes and scale adherence of plasma-sprayed coatings are summarized in Table IX. Unless otherwise noted, all the data were obtained from coatings produced by spraying fine powders at nominal feed rates of 8 pounds per hour, a power level of 22.5 KW, and application rates of 0.001 - 0.002 inch per pass. Coating thicknesses recorded in Table IX varied by no more than ± 0.5 mils from the intended values of 2.5, 4.5, and 6.5 mils.

The markedly superior oxidation behavior of coatings produced from fine powders is immediately apparent from the summary in Table IX. Quite high weight gains, accompanied by gross spalling, were observed in coatings produced from coarse powders under the least-severe air-oxidation conditions imposed (50-hour isothermal exposure at 2100°F). This behavior is associated with the rather high degree of porosity in such coatings, as noted above, which results in a large increase in the surface area of the sample in contact with air during exposure. The very large weight gains exhibited by coarse-powder coatings in air exposure can be reduced by short pretreatment in pure oxygen, as shown by comparison of the data from the 6.5-mil coatings of Cr-30% Y_2O_3; but, even after this preoxidation, some spalling occurs and the gross weight gain of 4.87 mg/cm^2 is higher than that of the base alloy under these air-exposure conditions. Preoxidation of the fine powder coatings is considerably more effective. Weight gains of about 3.5 mg/cm^2 were observed in 50-hour air exposure of 4.5-mil coatings of both Cr-30% Y_2O_3 and Cr-10% Y_2O_3 powders when they were tested in the sprayed and vacuum-annealed condition. After 2-hour preoxidation at 2000°F, the weight gains in air are well below 1 mg/cm^2, and the results are quite reproducible. Although weight gains in the preoxidation treatment of the specimens varied, reflecting minor differences in void contents and arrays, duplicate sets of specimens exhibited maximum variation of about 0.1 mg/cm^2 in subsequent 50- and 100-hour air exposures.

The oxidation screening tests summarized in Table IX demonstrate that lower volume fractions of Y_2O_3, within the range studied, resulted in more protective sprayed coatings. At equivalent thicknesses, there is a tendency toward higher weight gains and greater spalling as the oxide concentration in the Cr-Y_2O_3 layers is increased from 10 to 50%, due to the increased porosity associated with greater Cr-Y_2O_3 interface area as the Y_2O_3 content increases. The results also indicate that plasma-sprayed coating thicknesses of 4 to 5 mils afforded the greatest resistance to air oxidation. Coatings of 2 to 3 mils thickness, although they were generally adherent in both isothermal and cyclic oxidation, did not significantly reduce the weight gain characteristics of the substrate alloy. Sprayed coatings of 6- to 7-mil thickness were more protective than the thinnest coatings in isothermal air oxidation for the short duration, but were more subject to spalling during thermal cycling or after longer continuous exposure. The Cr-10% Y_2O_3 coating provided an exception to this trend, but the weight gain was considerably higher than that exhibited by the coating of intermediate thickness even in this case. Thus, these screening tests indicate that mixtures of 10 to 30 volume percent Y_2O_3

Table IX. Oxidation Behavior of Plasma-Sprayed Samples.

	Coating		Oxidation Weight Gain (mg/cm^2)			
				Isothermal		Cyclic
Desig	Y_2O_3 (Vol %)	Thick. (Mils)	2000°F O_2 2 Hrs	50 Hrs	100 Hrs	100 Hrs
O1	50	2.5	1.58A	2.26A	3.36A	4.81A
O2	50	4.5	1.62A	1.20A	4.55S	-
P1	50*	4.5	-	12.71S	-	-
P2	50	6.5	2.06A	1.85A	6.47S	-
Q	30	2.5	2.24A	2.10A	2.92A	3.85A
R1	30	4.5	1.39A	0.72A	0.91A	1.94A
R2	30	4.5	1.46A	0.85A	0.96A	2.01A
S	30	4.5	-	3.45B	-	-
T	30	6.5	1.98A	1.40A	2.63AS	3.20AS
U1	30*	6.5	-	15.40S	-	-
U2	30*	6.5	3.92B	4.87S	-	-
V	10	2.5	1.46A	2.08A	3.26A	4.06AS
W1	10	4.5	2.28A	0.76A	0.91A	1.27A
W2	10	4.5	1.60A	0.62A	0.88A	1.43A
X	10	4.5	-	3.52A	4.27AS	-
Y	10	6.5	1.73A	1.29A	2.80A	3.45A

* Coarse powders. All other sprayed with fine powders; see Table I

A = Adherent Oxide

S = Spalling Oxide

B = Blistered Oxide

in chromium, sprayed as fine powders to thicknesses of 4 to 5 mils, represented the most effective of the plasma-sprayed coating variations. Photomicrographs of these coatings after 100-hour air oxidation at 2100°F are shown in Figure 18. The scales are irregular but quite tenacious, with some penetration along grain boundaries. Particularly in the Cr-30% Y_2O_3 coating, the voids (which were originally randomly distributed through the sprayed coating) are concentrated and partially aligned near the coating-substrate interface. No evidence of nitridation was observed in either the coating or substrate, and the hardness of the recrystallized alloy (approximately 320 kg/mm^2) was unaffected by the oxidation exposure in the plasma-sprayed conditions shown. Hardness measurements in the sprayed coatings themselves were erratic, because of the porosity and the nonuniform distribution of the Y_2O_3 particles. In the sprayed-and-annealed condition, the microhardness measurements were in the range of 170 ± 40 kg/mm^2. After continuous and cyclic 100-hour air-oxidation exposures at 2100°F, this range was increased to 200 ± 40 kg/mm^2 and 220 ± 50 kg/mm^2, respectively. As mentioned above, however, no hardening of the substrate alloy was observed.

5.5 BEND DUCTILITY OF COATING COMPONENTS

The ductile-brittle transition temperatures (DBTT), measured as described in Section 4.2.4, are presented for selected chromided, lithided, and plasma-sprayed conditions, both before and after 2100°F air oxidation in Table X. The coating designations are the same as those employed in the tabulations of the deposition and oxidation characteristics of the respective components summarized in preceding sections of the report.

Note that, in each case, application of the coating results in an apparent decrease of the DBTT of the substrate alloy after vacuum annealing at 2000°F. This is a result of the lower hardness of the coatings compared to the substrate alloy and the bend-test technique which places maximum strain on the outer surface (where, in the coated samples, the ductility might be expected to be higher in view of the lower hardnesses and the associated lower yield strengths). Apparently there are thermal stresses generated in hot plasma spraying of cold specimens that require stress relief to remove, since the as-sprayed DBTT is considerably higher than that after the vacuum heat treatment. Such differences are not observed in the two metallided conditions, because the coating process is performed with the substrate and the deposit under isothermal conditions at elevated temperatures. It is also of interest that, after pretreatment in pure oxygen, the DBTT values of each of the coatings remain rather low, providing some evidence that oxygen is not primarily responsible for the large ductility losses that occur upon air exposure at elevated temperatures.

After air oxidation under the three screening conditions employed, the DBTT values correlate quite closely with the relative tenacity of the scales that was discussed in the three preceding sections. The most reproducible protectiveness is displayed by the plasma-sprayed coatings, provided

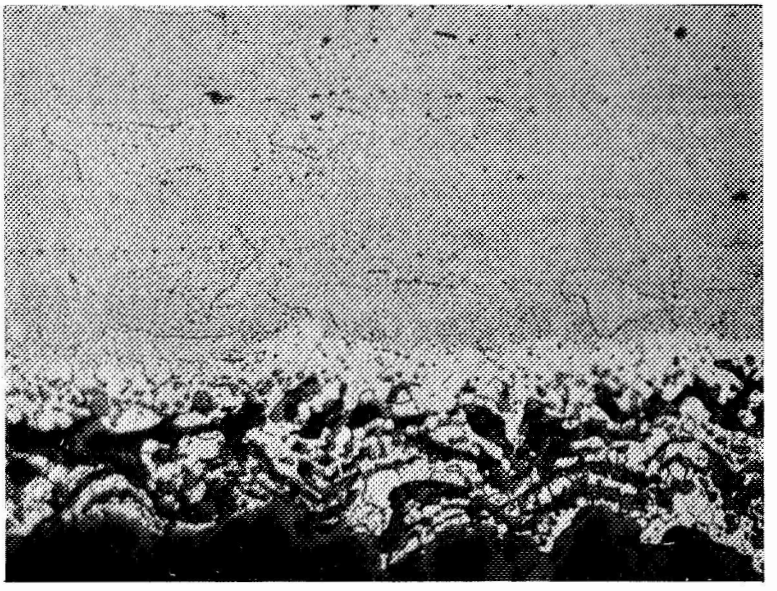

A. 10% Y_2O_3 Mt. E1662

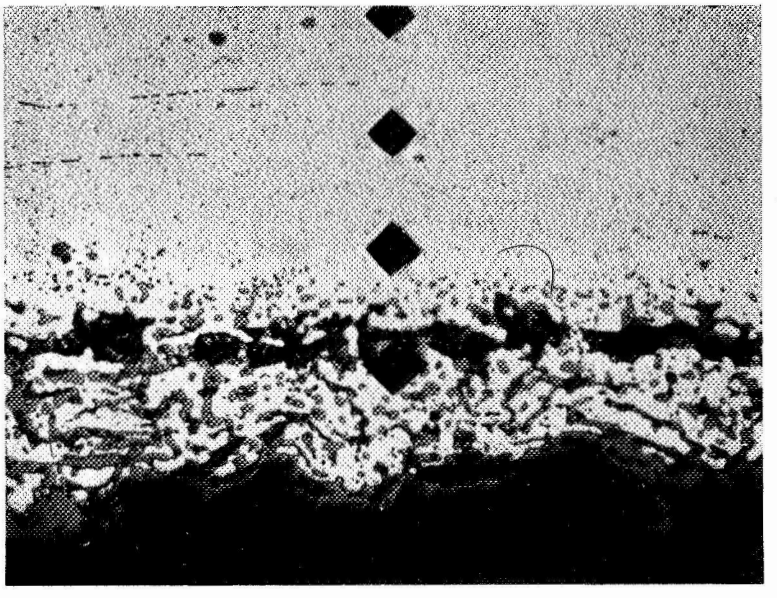

B. 30% Y_2O_3 Mt. E1665

Figure 18. Effects of 100-Hour Cyclic Air Oxidation at 2100°F on the Microstructure of 4.5 Mil Plasma-Sprayed Cr-Y_2O_3 Coatings (250X).

Table X. Effects of Coating and Pretreatments on Mechanical Properties in Bending.

Coating Designation	Condition	Test T (°F)	Fiber Stress (KSI)	Bend Angle (°)	Approximate DBTT[a] (°F)
Chromided (E)	As Coated	800	41.6	> 45	
	"	600	70.9	> 30	300
	"	400	82.5	> 15	
	"	200	102.6	1	
Chromided (E)	2000°F/2 Hrs/Vac	800	39.6	> 45	
	"	600	68.7	> 30	300
	"	400	86.0	> 15	
	"	200	92.1	0	
Chromided (E)	2000°F/2 Hrs/O_2	800	43.8	> 45	
	"	600	71.3	> 30	300
	"	400	88.4	> 15	
	"	200	101.0	0	
Lithided (K)	As Coated	800	37.2	> 30	
	"	600	59.1	> 15	500
	"	400	74.5	6	
Lithided (K)	2000°F/2 Hrs/O_2	800	38.8	> 15	650
		600	61.1	8	
Plasma, 30% Y_2O_3 (R)	As Coated	1000	47.3	> 30	
	"	800	67.8	> 15	700
	"	600	77.2	5.3	
Plasma, 30% Y_2O_3 (R)	2000°F/2 Hrs/Vac	1000	72.5	> 45	
	"	800	81.0	> 30	500
	"	600	83.2	> 15	
	"	400	85.1	6.2	
Plasma, 30% Y_2O_3 (R)	2000°F/2 Hrs/O_2	1000	39.8	> 45	
	"	800	67.0	> 30	500
	"	600	55.4	> 15	
	"	400	83.2	4	
Plasma, 30% Y_2O_3 (R)	200°F/200 Hrs Argon	1000	48.2	> 45	
	"	800	80.7	> 30	500
	"	600	88.3	> 15	
		400	87.5	8.5	

[a] Ductile-brittle transition temperature in bending over radius of 4t at ram speed of 1 ipm

that the preoxidation treatment is employed. Much slower heating rates are imposed in this pretreatment than in the air exposures, with the result that some spalling of the oxide (and plasma layer itself) occurs upon air oxidation of the as-sprayed coating (Condition S); and, partial embrittlement is observed after only 50 hours of isothermal exposure. The results in Table XI also confirm the oxidation measurements, in that increasing protectiveness results from decreasing the volume fraction of Y_2O_3 from 50 to 30 to 10%. It is of course possible that still lower volume fractions would have shown even greater superiority.

Of the two versions of metallided coatings (Cr and Li), chromiding alone appears to be significantly more protective, particularly under cyclic exposure conditions where all of the lithided specimens tested exhibited rather high weight gains and excessive spalling (Table VII). In addition, chromiding in the LiF-CrF_3 bath at low current densities, where trace amounts of Li are codeposited with the Cr, appears (from the DBTT response as well as the air oxidation behavior) to be the more reliable method.

5.6 EFFECTIVENESS OF MULTIPLE-COMPONENT COATINGS

Based on the properties of the individual components discussed above, several systems that combined two or all three of the coating steps were selected for evaluation. Although lithiding appeared to be detrimental in the earlier work, it was included in these more complex coatings, in order to determine if an overcoat of plasma-sprayed Cr plus Y_2O_3 might reduce the spalling tendencies of lithided layers. Coating deposition was performed in the same ways that have been described previously for the components. Results of screening oxidation tests, and the effects of air oxidation on the DBTT, are summarized in Tables XII and XIII. Letter designations in parentheses, as mentioned previously, refer to process parameters listed in Tables IV, VI, and VIII. Comparative oxidation behavior of the individual components is presented in Tables V, VII, and IX. As noted in Table XII, all samples in this series were preoxidized for 2 hours at 2000°F as the final step before air exposure, since all data obtained to this point indicate this step to be beneficial.

Both the oxidation data and the DBTT test results in Tables XII and XIII confirm the earlier observation that the trace quantities of Li incorporated during chromiding in the LiF-CrF_3 bath are far superior to lithiding per se. No further work was performed with lithided coatings. On the other hand, the duplex coatings (consisting of a chromided undercoat produced at low current density, with surface layers of about 4.5 mils of plasma-sprayed Cr containing 10 and 30 volume percent Y_2O_3) provide rather attractive protection against air embrittlement. As in earlier work, the lower volume fraction of Y_2O_3 produces the preferred results. With this coating, the DBTT of the Cr-Mo-TaC alloy substrate increases by less than 100°F under each of the three air exposure conditions investigated. Similar exposure of the base substrate results in a DBTT well above 1400°F, as shown in Table III. Thus, these duplex coatings, as well as the plasma-sprayed versions without an intermediate chromided layer, offer considerable protection against air embrittlement.

Table XI. Effects of Air Oxidation on the Bend Ductility of Selected Coatings.

Coating Designation	DBTT[(a)] After 2100°F, Air (°F): Isothermal 50 Hr	Isothermal 100 Hr	Cyclic 100 Hr
Chromided (G)	1050	-	-
Chromided (E)	725	750	850
Chromided (F)	700	-	775
Lithided (M)	> 1200	-	-
Lithided (K)	650	-	> 1200
Lithided (L)	775	800	1150
Plasma, 50% Y_2O_3 (O)	675	850	-
Plasma, 30% Y_2O_3 (R)	625	725	760
Plasma, 30% Y_2O_3 (S)[(a)]	875	-	-
Plasma, 10% Y_2O_3 (W)	600	650 - 700	625 - 700

(a) Ductile-brittle transition temperature in bending over radius of 4t at ram speed of 1 ipm

(b) Exposed to air without pretreatment in pure O_2. All others preoxidized at 2000°F, 2 hours

Table XII. Oxidation Behavior of Multiple-Component Coatings.

	Oxidation Weight Gain (mg/cm^2)			
		2100°F Air		
	2000°F O_2	Isothermal		Cyclic
	2 Hrs	50 Hrs	100 Hrs	100 Hrs
1. Chromided (E) 30% Y_2O_3 Plasma (R)	1.79A	1.08A	1.62A	1.54A
2. Chromided (E) Lithided (K) 30% Y_2O_3 Plasma (R)	1.42A	0.83A	-	6.25S
3. Chromided (E) 10% Y_2O_3 Plasma (W)	1.71A	0.67A	0.95A	1.18A
4. Chromided (E) Lithided (K) 10% Y_2O_3 Plasma (W)	1.10A	1.25A	-	5.90S

A = Adherent Oxide

S = Spalling Oxide

Table XIII. Effects of Air Oxidation on the Bend Ductility of Multiple-Component Coatings.

	DBTT After 2100°F Air (°F)		
	Isothermal		Cyclic
Coating	50 Hrs	100 Hrs	100 Hrs
1	650	750	725
2	1000	-	> 1200
3	625	600	675
4	850	-	1100

6.0 CRITICAL EVALUATION OF SELECTED COATINGS

Four coating systems were chosen for testing under more severe conditions. These four systems are nominally 4.5-mil layers of plasma-sprayed mixtures of Cr plus 10 volume percent and 30 volume percent Y_2O_3, sprayed over the bare substrate and over the chromided undercoats of approximately 0.8-mil thickness. Coatings were vacuum annealed for 2 hours at 2000°F after each step in the application cycle and were pretreated in purified O_2 for the same time and temperature prior to air exposure.

The additional factors that were investigated in this work are:

(1) The effects of extending the air oxidation time to 200 hours in both isothermal and cyclic exposures

(2) The effects of increasing the cooling rates and hence the thermal shock severity during cyclic testing

(3) The effects of intentional coating defects on the protectiveness of the coatings

Results of these tests are examined separately in the following sections.

6.1 RESPONSE TO 200-HOUR AIR OXIDATION AT 2100°F

Weight change characteristics measured in the isothermal and cyclic exposures, and the effects of these exposures on the DBTT, are summarized in Table XIV. Individual measurements recorded in air-oxidation and bend testing of the specimens are presented in Tables XV and XVI for the continuous and cyclic exposures, respectively.

The isothermal results confirm the earlier observation that the plasma-sprayed coating with 10 percent volume fraction of Y_2O_3 affords greater protection against embrittlement. The behavior of this coating applied over the Cr + Li undercoat (System B in the tabulations) is particularly attractive, with considerable ductility measured at 550°F using the multiple-bend technique and a full bend recorded at 650°F. Since the uncoated substrate has a DBTT of about 580°F after a 200-hour vacuum exposure at 2100°F, the effectiveness of this coating in isothermal oxidation is rather striking.

Results of the 200-hour cyclic oxidation, in which samples were rapidly cooled to room temperature three times in each 20-hour period, represent a quite different situation. Although the duplex 90 Cr - 10 Y_2O_3 coating sprayed over the Cr + Li metallided layer continued to demonstrate superiority over the other systems selected, the apparent DBTT of 850 to 900°F is a large increase over all the DBTT values measured after each of the other exposures imposed on this coating. Still higher DBTT results are indicated for the other three coating systems included in this portion of the study.

Table XIV. Effects of 200-Hour Air Oxidation at 2100°F on the Weight Change and Ductility of Selected Coatings.

Coating	Total Wt Change (mg/cm^2)		DBTT*(°F)	
	Isothermal	Cyclic	Isothermal	Cyclic
A. 10% Y_2O_3 Plasma	2.10	4.38	800	1150
B. Chromided + 10% Y_2O_3 Plasma	1.90	2.03	625	875
C. 30% Y_2O_3 Plasma	1.49	7.17	850	1175
D. Chromided + 30% Y_2O_3 Plasma	1.41	2.48	800	1050

* Ductile-brittle transition temperature for full bend over radius of 4t at ram speed of 1.0 ipm.

Table XV. Bend Test Results After Continuous Air Oxidation at 2100°F For 200 Hours.

	Coating System	Test T (°F)	Fiber Stress at Yield (KSI)	Deformation
A.	90Cr - 10Y_2O_3	1000	56.7	Full Bend
		950*	51.5	Ductile (> 45° Bend)
		900	53.2	Full Bend
		900	58.0	Fractured at 45° Bend
		850*	60.9	Ductile (> 30° Bend)
		800	64.1	Fractured at 5.2° Bend
		750*	63.7	Fractured at 4.5° Bend
B.	Metallided plus 90Cr - 10Y_2O_3	900	50.0	Full Bend
		800*	57.9	Ductile (> 90° Bend)
		800	54.3	Full Bend
		750*	-	Ductile (> 75° Bend)
		700	-	Ductile (> 60° Bend)
		700	52.3	Full Bend
		650*	-	Ductile (> 45° Bend)
		650	54.2	Full Bend
		650	58.5	Fractured at 29° Bend
		600*	-	Ductile (> 30° Bend)
		600	58.8	Fractured at 3.5° Bend
		550*	-	Fractured at 23° Bend
C.	70Cr - 30Y_2O_3	1000	58.7	Full Bend
		950	52.1	Full Bend
		900	63.3	Fractured at 8° Bend
		900	53.9	Full Bend
		850	53.5	Fractured at 37° Bend
		800	60.4	Fractured at 0° Bend
D.	Metallided plus 70Cr - 30Y_2O_3	1000	52.3	Full Bend
		950	53.6	Full Bend
		900	56.2	Full Bend
		900	62.5	Fractured at 9° Bend
		850	55.0	Full Bend
		800	65.2	Fractured at 8° Bend

* Multiple-bend specimen, deformed through 15° bend angle at successively lower temperatures as indicated. All others to full bend or fracture.

Table XVI. Bend Test Results After Cyclic Air Oxidation at 2100°F For 200 Hours.

	Coating System	Test T (°F)	Fiber Stress at Yield (KSI)	Deformation
A.	90 Cr - $10Y_2O_3$	1200*	36.0	Ductile (> 15° Bend)
		1100*	-	Fractured at 2.3 Bend
		1100	41.8	Fractured at 6° Bend
		1000	42.0	Fractured at 3.2° Bend
B.	Metallided plus 90Cr - $10Y_2O_3$	1100*	45.3	Ductile (> 80° Bend)
		1050*	-	Ductile (> 65° Bend)
		1000	55.8	Full Bend
		1000*	-	Ductile (> 50° Bend)
		950	59.0	Full Bend
		950*	-	Ductile (> 35° Bend)
		900*	-	Ductile (> 20° Bend)
		900	45.2	Fractured at 13.2° Bend
		900	-	Full Bend
		850	45.7	Fractured at 7° Bend
		850*	-	Ductile (> 15° Bend)
		800	-	Fractured at 5.2° Bend
C.	70Cr - $30Y_2O_3$	1200*	41.2	Ductile (> 20° Bend)
		1150*	-	Fractured at 5.7° Bend
		1100	33.7	Fractured at 4.2° Bend
		1000	33.8	Fractured at 3.5° Bend
D.	Metallided plus 70Cr - 30 Y_2O_3	1200*	42.1	Ductile (> 40° Bend)
		1150*	-	Ductile (> 40° Bend)
		1100	33.2	Full Bend
		1100*	-	Ductile (> 20° Bend)
		1100*	37.2	Ductile (> 40° Bend)
		1050*	-	Fractured at 6.4° Bend
		1050*	-	Ductile (> 28° Bend)
		1050	35.8	Fractured at 7.5° Bend
		1000*	-	Fractured at 11.2° Bend
		1000	37.8	Fractured at 6.5° Bend

* Multiple-bend specimen, deformed through 15° bend angle at successively lower temperatures as indicated. All others to full bend or fracture.

Behavior of Systems A and C (the plasma-sprayed coatings without the intermediate chromided layer) was not unexpected, since samples of both coatings exhibited extensive spalling during the latter stages of cycling. Spall-product weights as high as 30 mg/cm^2 are indicated in Table XVII for these systems, while the plasma-sprayed coatings applied over the Cr - Li undercoat show only small differences between net and gross weight changes, averaging about 0.3 mg/cm^2 for the 10% Y_2O_3 and 0.6 mg/cm^2 for the 30% Y_2O_3 versions. Some minor flaking of the oxide near the edges was noted; unlike the nonmetallided coatings, in no case was a large fraction of the coating missing from any area of the samples.

Nevertheless, the effect on the DBTT appears to be quite severe in extending the exposure time from 100 to 200 hours in cyclic air oxidation. The abrupt nature of the increase is indicated in the following summary of the effects of various exposures on the DBTT of the substrate alloy and of samples with the most effective Cr - Li plus 90 Cr - 10 Y_2O_3 coating:

Condition	2100°F Exposure	Approximate DBTT (°F)
Bare	200 hrs/vacuum	580 ± 20
Bare	200 hrs/air/isothermal	>> 1400
Bare	200 hrs/air/cyclic	>> 1400
Coated	200 hrs/vacuum	600 ± 25
Coated	50 hrs/air/isothermal	625 ± 25
Coated	100 hrs/air/isothermal	600 ± 25
Coated	200 hrs/air/isothermal	625 ± 25
Coated	100 hrs/air/cyclic	620 ± 50
Coated	200 hrs/air/cyclic*	875 ± 25
* Cooling rate increased in last 80 hours, see Section 6.2		

Probable reasons for the drastic effect of 200-hour cyclic oxidation are examined in the following section.

6.2 EFFECT OF COOLING RATE IN CYCLIC OXIDATION

In the course of conducting the cyclic oxidation tests, it was noted that when the rate of cooling from the oxidation temperature (2100°F) was increased, the overall rate of oxidation increased. The difference in cooling rates was achieved through the use of variable geometry support plates to hold the crucibles containing the test specimens. When thin ($\frac{1}{4}$-inch thick) alumina plates were substituted for 2-inch thick zirconia plates, specimen cooling rates increased as indicated in Figure 19. In order to determine the magnitude of the effect, a 200-hour test was conducted where both bare and coated specimens were exposed to the different cooling rates.

Weight change measurements recorded during cyclic exposure of coated and bare specimens are compared in Figure 20. The differences are even more striking for the bare substrate than for the coated samples. Average

Table XVII. Weight Changes in Cyclic 200-Hour Air Oxidation at 2100°F.

Coating		WEIGHT CHANGE (mg/cm^2) AT ELAPSED TIME OF:									
		Net	Gross	Net	Gross	Net	Gross	Net	Gross	Net	Gross
A. 90Cr - 10Y_2O_3	High	1.90	2.30	-5.15	4.90	-14.6	4.91	-21.8	3.54	-25.9	3.39
	Low	1.37	1.29	2.55	2.84	2.56	4.17	1.90	4.48	3.37	5.90
	Avg. (6)	2.25	2.50	-0.18	4.03	- 6.05	4.65	-10.7	4.60	-18.8	4.38
B. Chromided + 90Cr - 10Y_2O_3	High	1.44	1.69	1.55	1.76	1.71	1.88	1.98	2.28	2.32	2.76
	Low	1.19	1.32	1.19	1.42	1.27	1.38	1.22	1.46	1.42	1.68
	Avg. (6)	1.33	1.41	1.39	1.53	1.51	1.60	1.58	1.84	1.73	2.04
C. 70Cr - 30Y_2O_3	High	0.99	1.14	2.46	3.98	3.83	7.42	4.69	9.71	5.01	12.97
	Low	0.92	0.92	1.78	1.93	2.41	3.78	2.99	3.58	3.81	4.72
	Avg. (6)	0.98	1.06	2.01	2.40	3.03	4.17	3.64	5.00	4.65	7.17
D. Chromided + 70Cr - 30Y_2O_3	High	1.70	1.77	2.07	2.38	2.42	2.88	2.72	3.17	3.12	3.69
	Low	0.83	0.89	0.92	1.33	1.00	1.67	1.20	1.76	1.31	1.97
	Avg. (6)	1.05	1.13	1.26	1.73	1.42	2.00	1.62	2.18	1.88	2.48

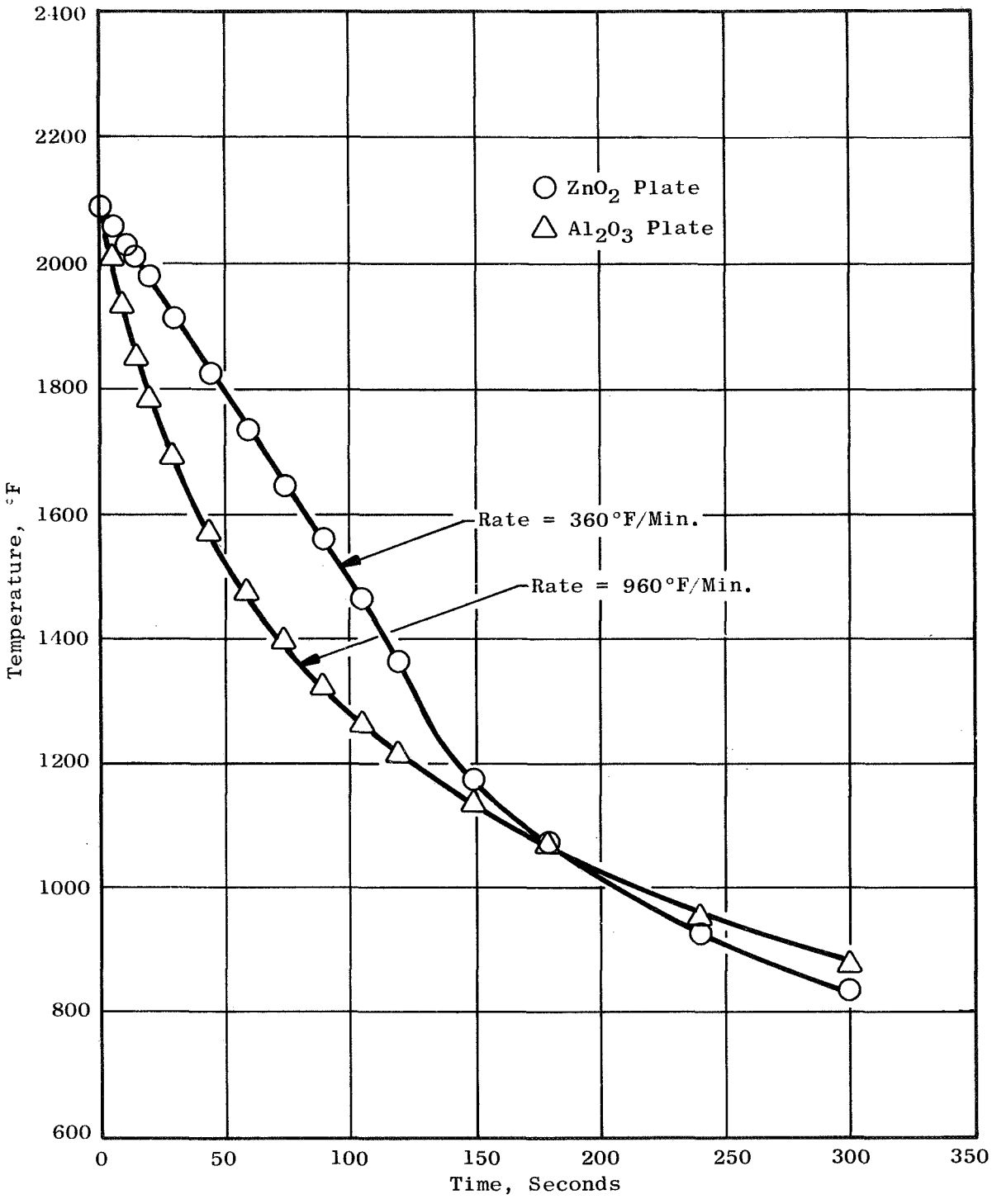

Figure 19. Specimen Cooling Curves - Related to Specimen Holders Used in the Cyclic Oxidation Tests.

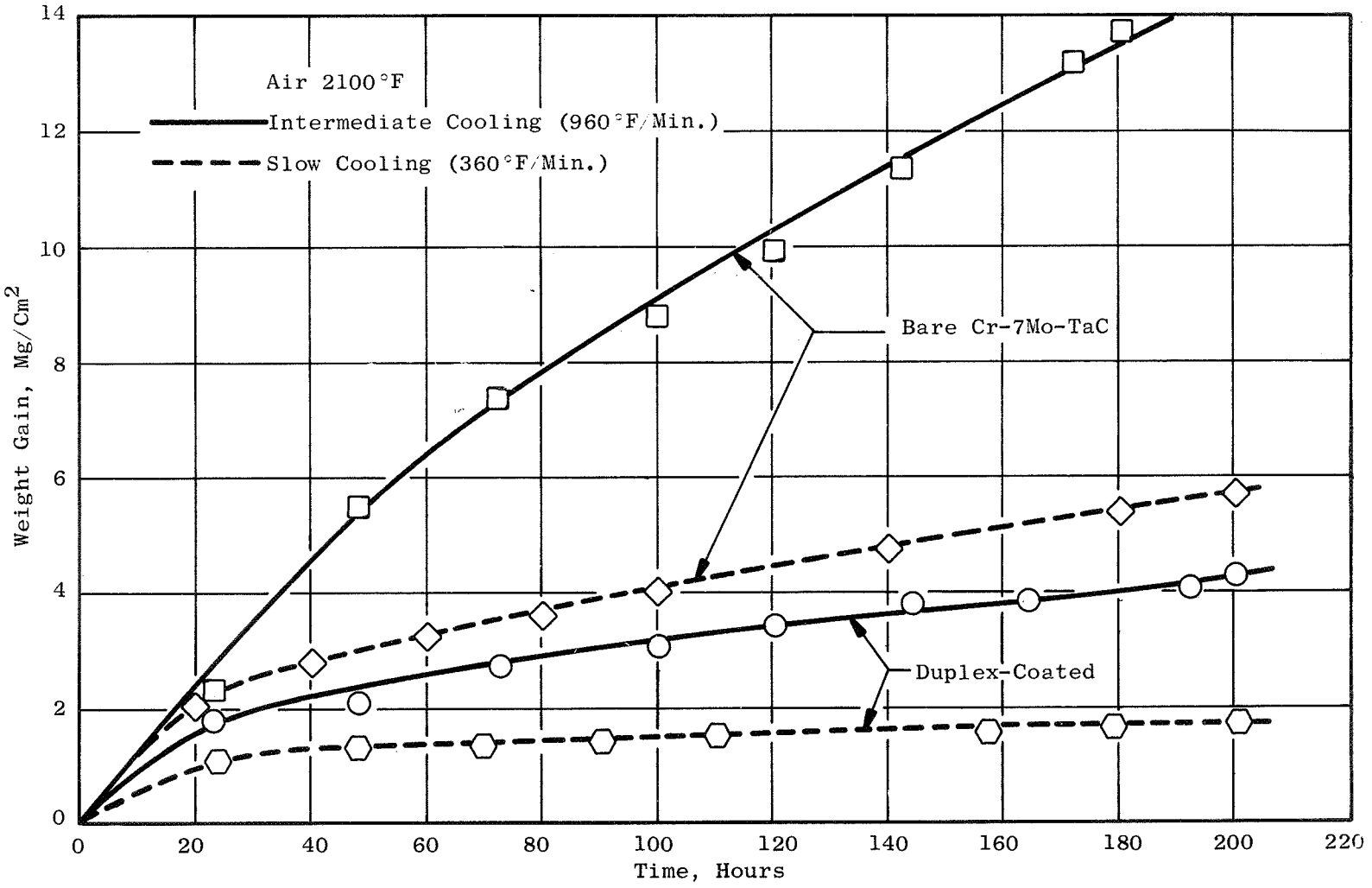

Figure 20. Effect of Cooling Rate on the Air Oxidation of Chromided Plus Plasma-Sprayed (90Cr-10Y_2O_3) and Substrate Alloy.

terminal weight gains in each instance are slightly more than doubled under the faster cooling rates; but, in the case of the bare substrate, this corresponds to an increase of over 8 mg/cm^2, while in the coated samples the increase is only about 2.5 mg/cm^2.

Photomicrographs of bare and coated samples after cyclic exposure under the two conditions are shown in Figure 21. Not only is much more spalling evident in oxide on the bare samples at the higher rate of cooling, but both coated and bare samples exhibit much more blistering of the oxide under these conditions. These observations, and the differences in weight gain kinetics noted above, suggest that the reason for the more severe attack under higher rates of cooling is the mismatch in the thermal expansion coefficient between Cr and Cr_2O_3, and the associated thermal stresses that are generated during rapid thermal transients which cause spalling of the protective oxide. Lower cooling rates induce a lower stress in the cooling as well as allow for relief of the stresses by plastic flow of either the substrate or the surface oxide at high temperatures. With high cooling rates, plastic flow will be minimized, thereby increasing the residual stresses. Most of the spalling is observed at edges of the coated samples. It would be at such sites that thermal stresses would have their largest effect. Tedmon[29] has discussed this point with respect to Cr_2O_3 scales on Fe - Cr alloys, and his comments are equally applicable to the scaling of Cr-base alloys. At 2000°F, the coefficient of thermal expansion of Cr_2O_3 is about 4.2×10^{-6} in./in. °F compared to 6.4×10^{-6} in./in. °F for Cr. Upon cooling, a scale (formed during oxidation of unalloyed Cr at 2100°F to room temperature, an unrelieved thermal strain of about 4.4×10^{-3} in./in.) would result. Using the elastic modulus of Cr for purposes of estimation, this strain could correspond to a stress of greater than 160,000 psi if it were competely unrelieved by plastic flow during cooling. Although the thermal gradients in the specimens of the present study are unknown, it is clear that rather significant stresses can be generated during rapid cooling.

Effects on the DBTT of the duplex coating of 100- and 200-hour cyclic air exposures at 2100°F, using the two cooling rates discussed above, are presented in Table XVIII. It is clear that it is the unintentionally-high rate of cooling that gives rise to the abrupt decrease in ductility noted in all of the coatings tested as described in Section 6.1 and not simply increasing the exposure time from 100 to 200 hours. The thin alumina plates were utilized in the last 80 hours of the tests reported in the listing on Page 64.

Some of the spalling observed in rapid cooling of the duplex coating is probably due to the porosity in the plasma-sprayed layer. Greater protection should therefore result if a method of producing a higher-integrity Cr-Y_2O_3 mixture can be devised, as it undoubtedly can be. In other systems, excellent oxide adherence is obtained in the presence of large differences in thermal expansion, coefficients of substrate, and surface oxide. The Fe Cr Al Y alloy is an example where excellent adherence of an Al_2O_3 surface oxide is obtained as a result of the presence of Y. Future effort should

Bare Substrate

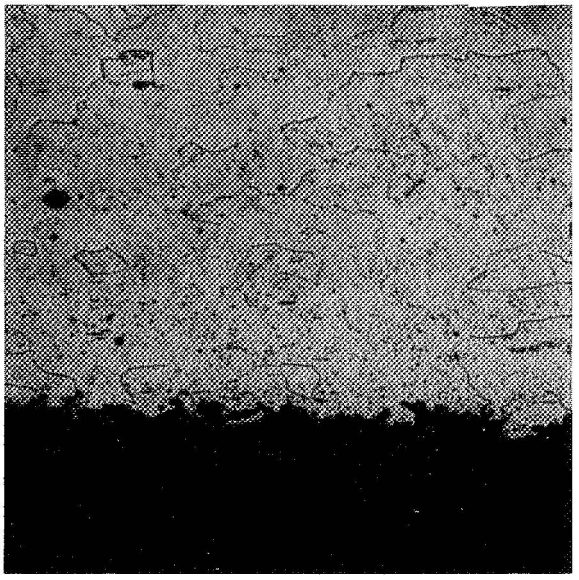

A. Cooled 360°F/Min. Mt. A8575

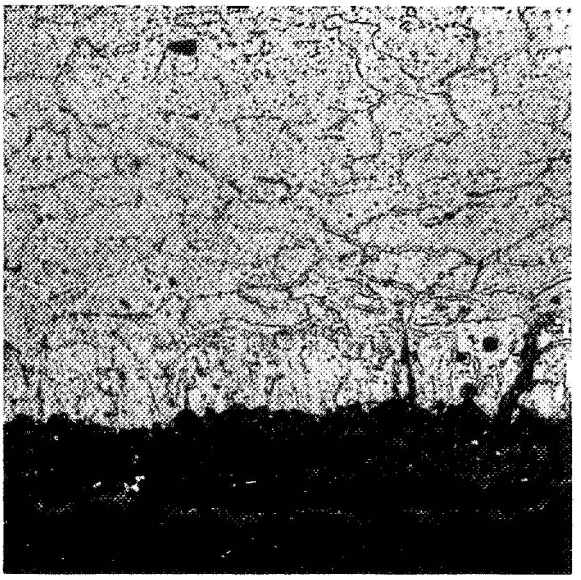

B. Cooled 960°F/Min. Mt. A9068

Duplex-Coated Substrate

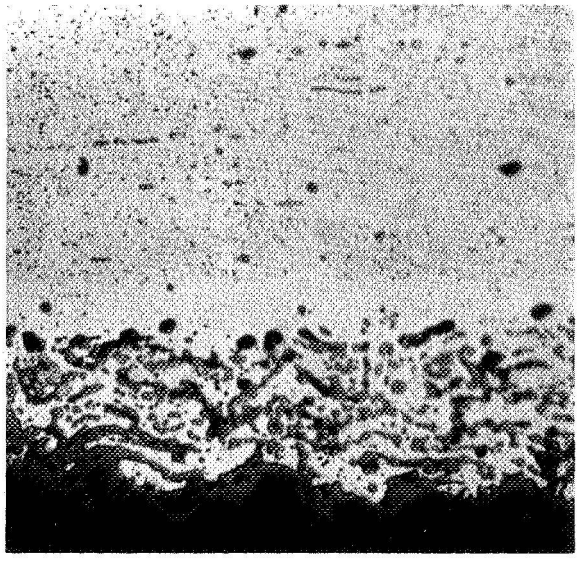

C. Cooled 360°F/Min. Mt. E1686

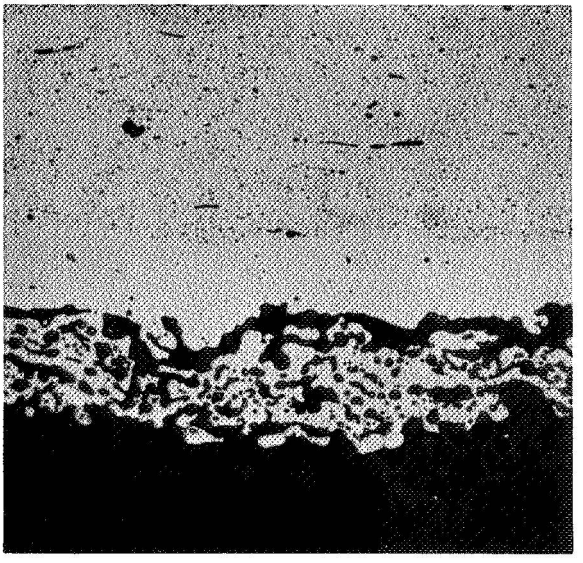

D. Cooled 960°F/Min. Mt. E1617

Figure 21. Effects of Cooling Rate in 200-Hour Cyclic Air Oxidation at 2100°F on the Structure of Bare and Duplex-Coated (Chromided +90Cr-10Y_2O_3) Cr-7Mo-TaC Alloy (250X).

Table XVIII. Effect of Cooling Rates in Cyclic Air Exposure on the Ductility Retention of Chromided Plus Plasma-Sprayed (90Cr-10Y_2O_3) Samples.

2100°F Air Exposure	Cooling Rate (°F/Min)	Time (Hrs)	Gross Wt Gain (mg/cm^2)	Approx DBTT (°F)
None	-	-	-	580
Isothermal	-	100	0.95A	600
Isothermal	-	200	1.90A	625
Cyclic	360	100	1.47A	675
Cyclic	360	200	1.76A	650
Cyclic	960	100	3.06B	925
Cyclic	960	200	4.30BS	950

A = Adherent Oxide

B = Blistered Oxide

S = Spalling Oxide

be aimed at obtaining improved scale adherence under cyclic conditions. In turbomachinery, the thermal cycles are much more rapid than those studied in this program.

6.3 EFFECTS OF INTENTIONAL DEFECTS

After the final pre-exposure in pure oxygen at 2000°F, intentional defects were made in specimens of each of the four selected coatings. These were made to a depth 0.002 inch below the coating/substrate interface by hardness impressions using a conical diamond indenter with an included angle of 30 degrees. The impressions, the intended depth of which were controlled by measuring the apparent diameter at the coated surface, were placed 0.100 inch and 0.200 inch on either side of the transverse center line of the samples on the side to be placed in tension during testing. Since these locations are displaced from the center line by less than the radius of the bending ram, each site was strained in the test.

Most of the intentional-defect specimens were tested under the cyclic conditions described in Section 6.1, where an unintentionally-high cooling rate was applied mid-way through the 200-hour cyclic exposure sequence. Weight change characteristics in each coating were identical, within the limits of scatter, with their nondefective counterparts shown earlier in Table XII. Values of the DBTT, measured by the multiple-bend technique described earlier, are compared for as-coated and intentional-defect specimens in the following listing:

	DBTT (°F) After 2100°F/200 Hrs/Cyclic	
	As-Coated	Intentional-Defect
A. 90 Cr - 10 Y_2O_3 Plasma	> 1100	> 1100
B. Metallided Cr-(li) 90 Cr - 10 Y_2O_3 Plasma	875	900-950
C. 70 Cr - 30 Y_2O_3	> 1200	> 1100
D. Metallided Cr-(Li) 70 Cr - 30 Y_2O_3 Plasma	1050	> 1100

The effect of the intentional defects, if any, are relatively small and are of much less consequence than the increased cooling rate applied in the sixth 20-hour period. Unfortunately, there were insufficient specimens available to permit a repeat of this cyclic test series under a constant rate of cooling. Results of 200-hour isothermal 2100°F air exposures on as-coated and intentional-defect samples of the four coatings are presented in Table XIX. From these data, it is evident that the small conical defects have essentially no effect on the protectiveness of the coating. If the Cr_2O_3 formed on the surfaces remains intact during service, the duplex-chromided plus plasma-sprayed Cr-Y_2O_3 system, particularly at 10 volume percent Y_2O_3, is an effective coating. Its shortcoming is its response to cyclic cooling at or above the highest cooling rate employed in this work.

Table XIX. Effect of Coating Defects on the Response of Selected Coatings To Isothermal Air Oxidation At 2100°F.

	Coating	Avg 200-Hr Wt Gain (mg/cm^2)		Approximate DBTT (°F)	
		As-Coated	Defected	As-Coated	Defected
A.	90Cr - $10Y_2O_3$	2.10	2.40	800	775
B.	Chromided + 90Cr - $10Y_2O_3$	1.90	1.82	625	625
C.	70Cr - $30Y_2O_3$	1.49	1.73	850	825
D.	Chromided + 70Cr - $30Y_2O_3$	1.41	1.51	800	750

7.0 SUMMARY AND CONCLUSIONS

The "Stabilized Cr_2O_3" coating approach for the protection of Cr-base alloys against embrittlement during air exposure at elevated temperature was evaluated in this work. Stabilization was achieved by adding monovalent Li (which was shown to greatly reduce the parabolic oxidation rate constant) and by incorporating Y_2O_3 particles in the surface (which were shown to not only promote scale adherence but also to reduce the oxidation kinetics from parabolic to near quartic). Under isothermal exposure conditions, or under cyclic conditions with moderate rates of cooling, an effective coating was demonstrated. Because of the rather large thermal expansion mismatch between Cr and Cr_2O_3, however, excessive blistering of the oxide occurred in a relatively few heating-cooling cycles when a high initial cooling rate of 960°F per minute from the air exposure temperature of 2100°F was applied. When such cyclic testing was continued for 200 hours, the original DBTT of about 580°F was increased to 900°F. Although this coating thus appears to be superior to any other coating yet reported for Cr-base alloys, its resistance to thermal cycling must be improved before it can be considered adequate for the severe service conditions of a jet engine environment.

REFERENCES

1. W.C. Hagel, "Factors Controlling the High Temperature Oxidation of Chromium", Trans. ASM 56 (1963) p. 583.

2. D. Caplan, A. Harvey and M. Cohen, "Oxidation of Chromium at 890-1200°C", Corrosion Sci. 3 (1963) p. 161.

3. G.R. Wilms and T.W. Rea, "Scaling of Chromium in a Hot Gas Stream", J. Less Comm. Met. 3 (1961) p. 234.

4. G.R. Wilms and T.W. Rea, "Loss of Metal from Chromium at Elevated Temperatures in Air", J. Less Comm. Met. 1 (1959) p. 411.

5. J.W. Clark, "Preparation and Properties of a Carbide-Strengthened Cr-W-Y Alloy (C-207)" General Electric Report R64FPD119, April, 1964.

6. D. Caplan and M. Cohen, "The Volatilization of Chromium Oxide, J. Electrochem. Soc. 108 (1961) p. 438.

7. C.S. Tedmon, Jr., "The Effect of Oxide Volatilization on the Oxidation Kinetics of Cr and Fc-Cr Alloys" J. Electrochem. Soc. 113 (1966) p. 766.

8. W.H. Smith and A.U. Seybolt, "Ductile Chromium", J. Electrochem. Soc. 103 (1966) p. 347.

9. B.C. Allen, D.J. Maykuth and R.I. Jaffee, "Influence of Impurity Elements Structure and Prestrain on Tensile Transition of Chromium "NASA Technical Note D-837, April, 1961.

10. H.L. Wain, F. Henderson, S. T.M. Johnstone and N. Louat, "Further Observations on the Ductility of Chromium" J. Inst. Metals 86 (1957-58) p. 281.

11. D.J. Maykuth, W.D. Klopp, R.K. Jaffee and H.B. Goodwin, "A Metallurgical Evaluation of Iodide Chromium" J. Electrochem. Soc. 102 (1955) p. 316.

12. R.E. Hook, H.J. Garrett and A.M. Adair, "The Occurrence and Partitioning of Impurity Phases in Recrystallized Chromium" Trans. Met. Soc. AIME 227 (1963) p. 145.

13. S.T.M. Johnstone, F. Henderson and H.L. Wain, "Heat Treatment and the Ductility of Chromium" J. Inst. Metals 88 (1959-60) p. 145.

14. J.W. Clark, "Development of High-Temperature Chromium Alloys" Final Report No. NASA CR-72731, November, 1970.

15. J.E. Fox and J.A. McGurty, "Chromium and Chromium-Base Alloys" p. 207 in Refractory Metals and Alloys, Interscience, New York, 1961.

16. C.S. Wukusick, "Research on Chromium-Base Alloys" ASD Technical Documentary Report 63-493, June, 1963.

17. C.E. Lundin, "Rare Earth Metal Phase Diagrams" Chap. 16 in the Rare Earths, John Wiley and Sons, New York, 1961.

18. A.U. Seybolt, "Nitrification and Oxidation-Resistant Chromium-Base Alloys" General Electric Report 65-RL-4010M, July, 1965.

19. A.U. Seybolt, "High-Temperature Oxidation of Chromium Containing Y_2O_3 Corrosion Science 6 (1966) p. 263-69.

20. C.S. Tedmon, Jr. and W.C. Hagel, "Electrochemical Formation of Lithium Alloys from Molten Lithium Fluoride" J. Electrochem. Soc. 115 (1968) p. 151-57.

21. C.S. Tedmon, Jr., and W.C. Hagel, "The Oxidation of Lithided Chromium" J. Electrochem. Soc. 115 (1968) p. 147-51.

22. W.C. Hagel and A.U. Seybolt, "Cation Diffusion in Cr_2O_3" J. Electrochem. Soc. 108 (1961) p. 1146.

23. W.A. Fischer and G. Lorenz, "Electrical Resistance and Thermoelectric Power Measurements in Cr_2O_3 up to 1750°C" Archiv. f. d. Eisen. 28 (1957) p. 497.

24. W.C. Hagel, "Electrical Conductivity of Li-Substituted Cr_2O_3" J. Appl. Phys. 36 (1965) p. 2586.

25. J.R. Stephens and W.D. Klopp, "Exploratory Study of Silicide, Aluminide, and Boride Coatings for Nitridation/Oxidation Protection of Chromium Alloys", Trans. Met. Soc. AIME., 245 (1969) pp. 1975-1981.

26. N.C. Cook, US Patent 3,024,175 through 3,024,177 March, 1962; US Patent 3,232,853 February, 1966.

27. E.R. Slaughter et al "Small Quantity Production of Complex Chromium Alloy Sheet", NASA CR-72545, December, 1968.

28. J.W. Clark, "Properties of Dilute, Carbide-Strengthened Chromium Alloys", General Electric Report R62FPD285, February, 1963.

29. C.S. Tedmon, Jr., "High-Temperature Oxidation of Fe-Cr Alloys in Composition Range of 25-95% Cr", J. Electrochem. Soc. 114 (1967) p. 788-95.